Xeroderma pigmentosum group F protein binds to Eg5 and functions in mitosis: Implications for XP-F

色素性乾皮症 F 群蛋白質はキネシン Eg5 と結合し、細胞分裂に寄与する: XP-F 群患者の病態との関連性

大阪大学大学院生命機能研究科

個体機能学講座　田中研究室

麗晶　陳

Li-Jing Tan

2011 年　3　月

Xeroderma pigmentosum group F protein binds to Eg5 and functions in mitosis: Implications for XP-F

色素性乾皮症 F 群蛋白質はキネシン Eg5 と結合し、細胞分裂に寄与する: XP-F 群患者の病態との関連性

大阪大学大学院生命機能研究科

個体機能学講座　田中研究室

麗晶　陳

Li-Jing Tan

2011 年　3　月

CONTENTS

ACKNOWLEDGEMENT

I would like to thank Prof. Kiyoji Tanaka for his insurmountable support during my graduate training. I strongly believe that under his mentorship, I received the best academic and research training, which will help me through and beyond my graduate study. I would like to acknowledge the Tanaka group staffs, Assoc. Prof. Masafumi Dr. Saijo, Dr. Katsuyoshi Horibata, Dr. Takashi Narita and Dr. Mineaki Seki who were continuously supportive and available for weekly meetings (seminar progress) and offering suggestions for improvement. I have greatly enjoyed working with all the graduate students in Tanaka lab. Their critical inputs and sharing of scientific thinking have made my experiments and research more reliable. Also not forgetting Tanaka lab's secretary Ms. Yoko Hirooka. I would like to thank my beloved parents. Knowing that I have their support and encouragement to pursue my study overseas helped me overcome the feelings of being far from home and establish a balance in my loyalties to Malaysia and Japan. I am indebted to the Ministry of Education, Culture, Sports, Science, and Technology, Government of Japan: MEXT for supporting my graduate study at Osaka University under the Japanese Government Monbukagakusho: MEXT Postgraduate Scholarship. This work was supported by a Grant-in-Aid for Scientific Research on Innovative Areas from the Ministry of Education, Culture, Sports, Science and Technology of Japan, and Health and Labor Sciences Research Grants for Research on Intractable Diseases (to KT). Lastly, I would like to thank Dr. Munehiro Asally and Prof. Yoshihiro Yoneda for providing the pEGFP c1 vector plasmid. I also thank Assoc. Prof. Laura Niedernhofer for kindly providing XP42RO and XP51RO hTERT cells.

General Introduction

Nucleotide excision repair (NER) mechanism

Nucleotide excision repair (NER) is a key DNA repair mechanism, and conserved in both prokaryotes and eukaryotes. However, NER mechanism is complex in eukaryotes and requires the action of more than thirty proteins in a sequential manner. NER pathway removes damaged DNA strand and replaces with a repaired DNA. The first step in NER is damage recognition. The types of DNA damage determine the fates of damage recognition either by global genome repair (GGR) (XPC, Rad23B, DDB complex and XPE) or transcription-coupled repair (TCR) (RNA polymerase II, CSA and CSB). In GG-NER, the XPC/hHR23B protein complex is responsible for the initial detection of damaged DNA. Conversely, damage recognition during TC-NER occurs when the transcription machinery is stalled at the site of DNA damage. The following steps involved are opening of the DNA strands around the damaged site by NER complex formation consist of XPC, Rad23B, XPB, XPD and TFIIH complex. Prior to excision, XPA, the heterotrimetric RPA and TFIIH are responsible to verify the DNA damaged site. The repair endonucleases XPF-ERCC1 and XPG are responsible to excise at 5' and 3' of the damaged DNA strand, respectively. Subsequently, DNA synthesis is carried out by DNA polymerase; polδ, polε and polκ, PCNA, XPG and several replication factors to fill in the gap. Finally the repaired DNA strand is sealed by DNA ligases (either DNA ligase I or III and XRCC1), which completes the NER process (Oogi *et al,* 2010) (Figure 1).

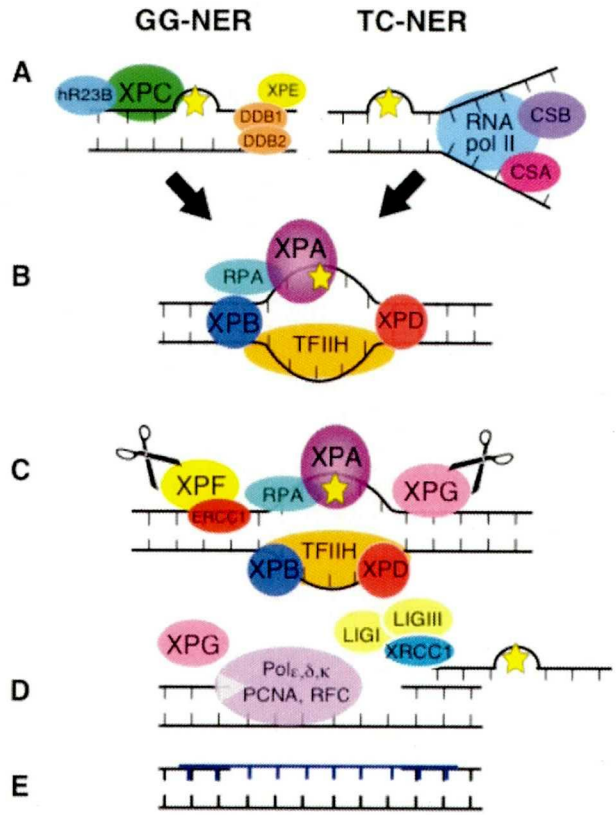

Figure 1. Nucleotide excision repair (NER) pathway (A) DNA damage recognition either by Global Genome Repair (GG-NER) or Transcription Coupled Repair (TC-NER) (B) Local unwinding at the damaged site (C) Dual incision of the damaged strand (D) Repair synthesis and strand ligation (E) Repaired DNA double strands.

XPF-ERCC1, one complex with two diseases

Defect in NER can leads to three prominent DNA repair diseases xeroderma pigmentosum (XP), Cockayne syndrome (CS) and trichothiodystrophy (TTD). My primary focus is in XP disease, which is characterized by severe photosensitivity, high incidence of skin cancers, severe skin pigmentation, and neurological disorders. Although XP is a rare, inheritable disease hence it appears to be present throughout the

world and every ethnic group. There are approximately 1 in 250 000 diagnosed case in Europe and United States (Friedberg *et al*, 2006). In Japan, the statistic is as high as 1 in 40 000 (Takebe *et al*, 1977). There are seven complementation groups of XP (XP-A through XP-G) and a variant XP-V. XP-A is classified as severe XP while XP-F as milder XP (Figure 2).

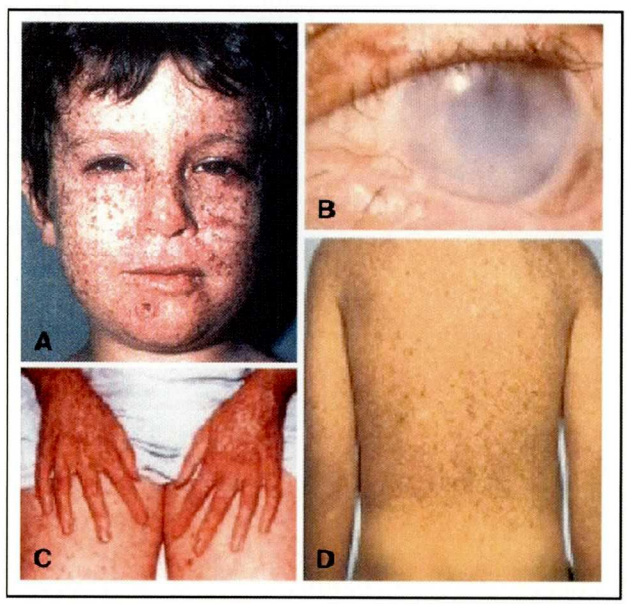

Figure 2. (A to D) Xeroderma pigmentosum (XP) patients and clinical symptoms. High incidence of skin cancers, hyperpigmentation, skin and eyes abnormalities.

My interest lies in the XP group F (XP-F). Mutations in XPF or ERCC1 render patients mild susceptibility to skin cancers, neurological abnormality, and a mild sensitivity to ultraviolet (UV) irradiation and DNA crosslink agent, mitomycin C (MMC). Recently, a patient named as XFE (*XPF-E*RCC1) was diagnosed with severe

XP phenotype, growth retardation and progeria syndrome (Niedernhofer *et al,* 2006) (Figure 3B).

In addition, the first identified ERCC1 patient, 165TOR was reported with severe cerebro-oculo-facio-skeletal (COFS) syndrome, mild XP phenotypes and severe developmental defects (Jaspers *et al,* 2007) (Figure 3C). *Xpf* or *Ercc1* knockout or mutant mice displayed same fate as the human XFE and ERCC1 patient cases (Tian *et al,* 2004) (Figure 3D). While wild type and *Xpa* knockout mice showed similar phenotypes in term of body size and weight (Figure 3E). Hence, XPF-ERCC1 is essential for normal cell function, growth and development.

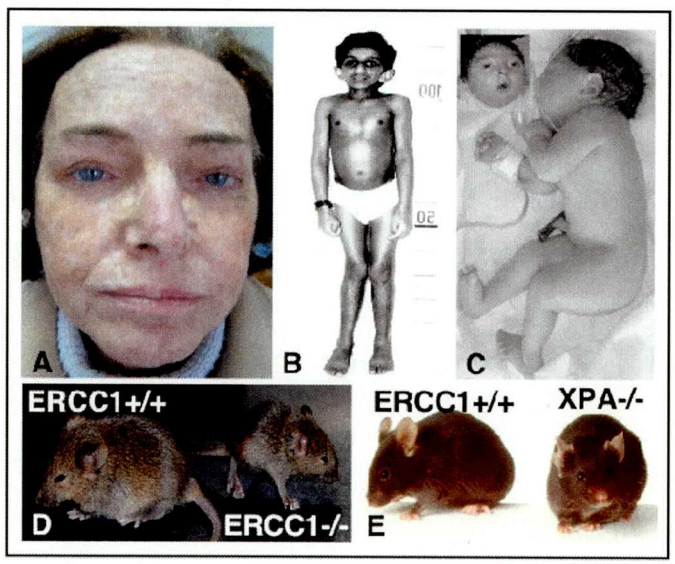

Figure 3. (A) Xeroderma pigmentosum group F (XP-F) patient (B) *XP*F-*E*RCC1 (XFE) with progeria, severe XP and neurological abnormality (C) ERCC1 patient (16TOR) (D) Wild type and *Ercc1* knockout mice (E) Wild type and *Xpa* knockout mice.

XPF-ERCC1 is a multifunctional complex involved in DNA repair and other functions

Since first identified more than thirty years ago, XPF-ERCC1 has become a prominent structure specific endonuclease in the repair pathway. The complex plays essential roles in NER, DNA intrastrand crosslink (ICL), double strand break (DSB), and homologous recombination (HR) repair (Kuraoka *et al,* 2000; Bhagwat *et al*, 2009). The versatility of XPF extends beyond repair pathway to telomere maintenance, immunoglobulin

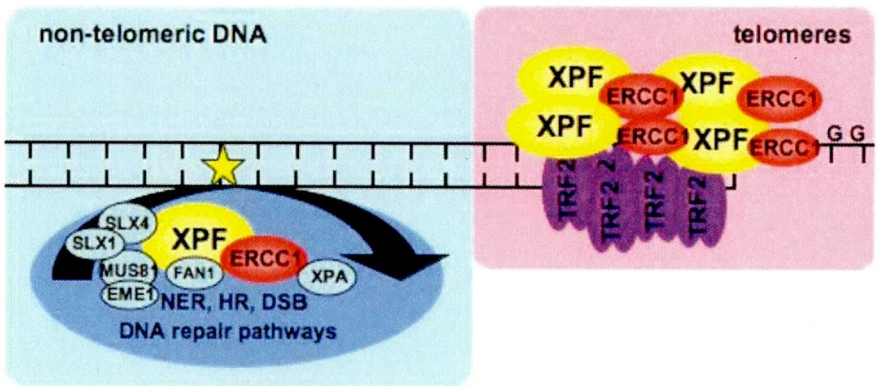

Figure 4. XPF is a multisubunit and multifunctional protein complex. (Left) In non-telomeric DNA, XPF-ERCC1 interacts with multiple binding partners, XPA, SLX1-SLX4, MUS81-EME1 and FAN1 to function in various DNA repair pathways, nucleotide excision repair (NER), homologous recombination (HR) and double strand break (DSB) repair. (Right) In the telomere region, XPF binds to TRF2 to regulate telomere maintenance independent of its nuclease activity.

switching and as predicative markers for chemotherapy (Zhu *et al,* 2003; Arora *et al,* 2010; Schrader *et al,* 2004).

The heterodimeric XPF-ERCC1 has emerged as a multifunctional complex with multiple roles in cells as evidenced by its interaction with many binding partners (Figure 4). However, it remains unclear whether XPF-ERCC1 acts independently or engaged with multiple binding partners when conducting its repair function. I set to investigate the mechanism underlying the multifunctional roles of XPF-ERCC1 by identifying an XPF-ERCC1-interacting protein. By performing affinity purification and mass spectrometry analysis of the XPF protein, I identified the kinesin protein Eg5/Kif11/THRIP (Eg5). Eg5 is responsible for the formation and separation of the centrosome and spindle pole during pre- and post-mitosis (Sawin & Mitchison, 1995).

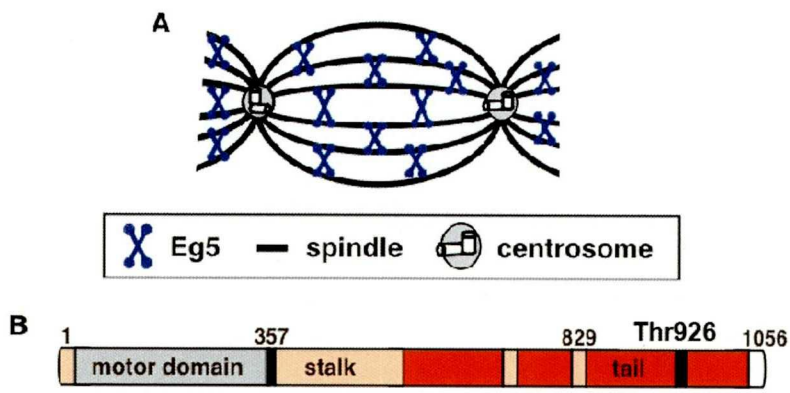

Figure 5. (A) Eg5 (tetramer) binds to the bipolar spindle during M phase (B) Schematic presentation of full length Eg5 (1-1056 amino acids) and a phosphorylation site, Thr926.

Phosphorylation of Eg5 at Thr926 is essential for Eg5 binding to the bipolar spindle and microtubules during M phase (Blangy *et al*, 1995) (Figure 5). Although the function of Eg5 during M phase has been well studied in species ranging from *Xenopus laevis* to human but the mechanisms that regulate Eg5 in the cell cycle remain elusive (Sawin & Mitchison, 1995). In fact, Eg5 has been correlated to cancer, leading researchers to target Eg5 inhibitors as potential anti-cancer drugs (DeBonis S *et al*, 2003). Moreover, the expression of Eg5 in various cancer cells can help predict a patient's survival in response to chemotherapy (Saijo T *et al*, 2006), which is similar to XPF-ERCC1 role as predicative marker in response to platinum based chemotherapy and survival (Arora S *et al*, 2010; Olaussen KA *et al*, 2006). It is plausible to speculate that XPF and Eg5 may involve in the same functional pathway that renders cancer cells resistance to chemotherapy.

Here, I demonstrated that Eg5 was co-purified with Flag-tagged XPF and endogenous XPF by immunoprecipitation in mammalian HEK 293 and HeLa cells, as well as in bacterial, *E. coli* systems. Both mass spectrometric and reciprocal immunoprecipitation results verified that XPF interacts with Eg5 by binding through the N-terminal region of XPF. XPF mutants mimicking XP-F patients showed binding with Eg5 as well for XPF mutant void of nuclease domain. This suggests that XPF-Eg5 interaction is independent of repair nuclease activity. Since Eg5 is a bipolar motor protein, I seized this opportunity to investigate XPF localization during M phase. In addition, I compare localization pattern between the wild type (WT) and mutant XPF (R799W, mild and R153P, severe). From my observation, I witnessed for the first time

GFP-R153P translocated to cytoplasm region during interphase (Figure 6D), while GFP-R799W and wild type GFP-XPF remained intact in nuclear region (Figure 6B and C). Mutation in R153P was located at the nuclear localization signal region of XPF and resulted in XPF mistranslocation. During M phase, WT and mutant XPF were observed in the cells but negative for empty vector, pEGFP (Figure 6A). Immunofluorescence staining reveals dynamic subcellular colocalization of XPF and Eg5 during M phase. Next, to define the localization of XPF and Eg5, knockdown of XPF in normal fibroblast, WI38VA13 cells were performed by siRNA transfection. XPF depleted cells displayed sensitivity to UV and MMC treatment. Depletion of XPF also induces cells with abnormal nuclear morphology, aberrant centrosome numbers, mitotic chromosome and segregation. These phenotypes were reverted by introducing WT-XPF into XPF-deficient cells (XP-F patient fibroblast cells). Expression of mutant XPF in the XP-F patient cells showed substantial recover from the phenotypes. These results support the notion that loss of XPF function led to chromosomal instability, which may help explain in part the close functional relationship between XPF and Eg5.

Taken together our results demonstrated that XPF have a cell cycle related subcellular localization, suggesting a role in coupling cell cycle and genome stability.

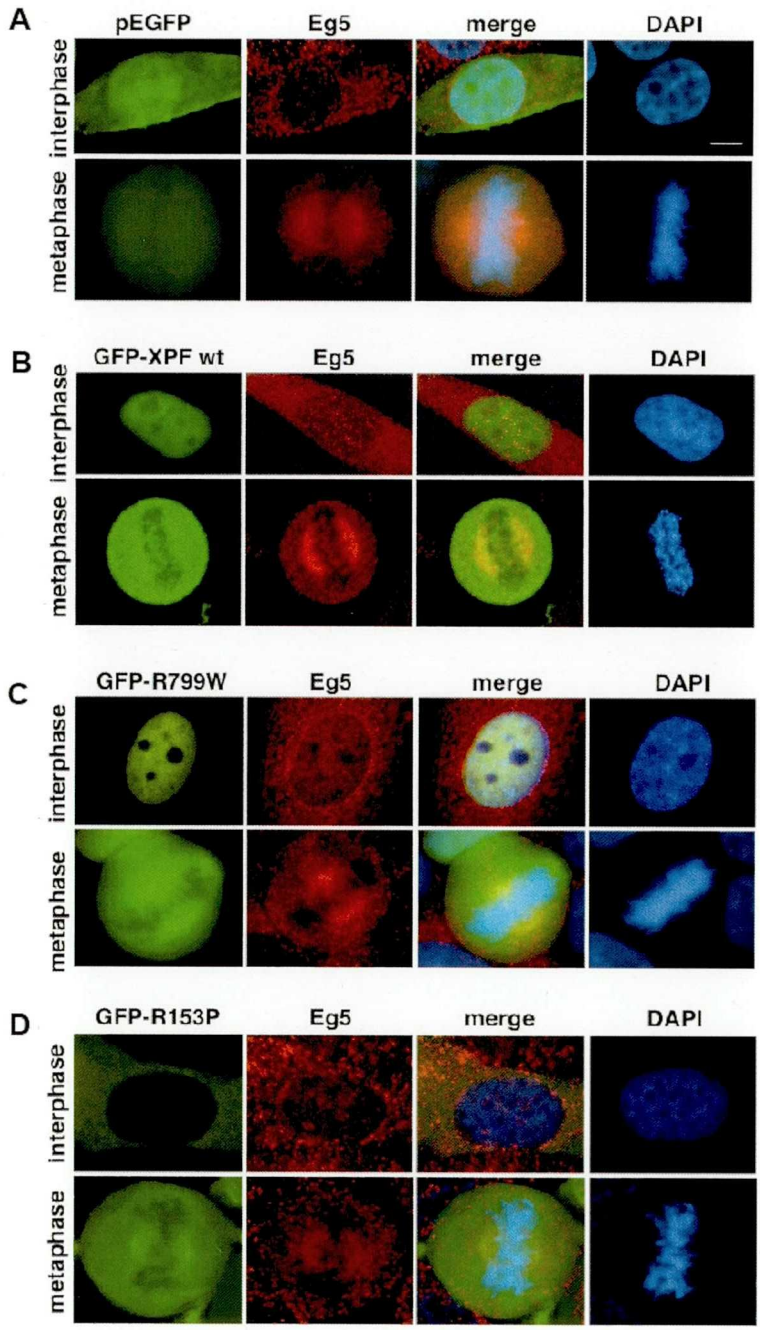

Figure 6. Localization of wild type and mutants GFP-tagged XPF in HeLa cells. Cells were subjected to immunofluorescence using of anti-Eg5 with during interphase and metaphase. (A) Empty vector, pEGFP (B) GFP-XPF wild type (C) GFP-R799W (D) GFP-R153P. Scale bar, 10 μm.

DNA repair and genome instability - The genotype and phenotype relationships of NER syndromes (XPC, XPD/CS and XPF/progeria)

In the recent years, there has been an increasing interest in the study of DNA repair proteins that associate with cell cycle and centrosome regulatory mechanism. For instance, GG-NER damage recognition factors, XPC and Rad23 form a heterotrimeric complex with centrosomal protein, centrin 2 (Araki *et al,* 2001). However, centrin 2 roles in damage recognition remain poorly understood. On the other hand, XPD forms three different complexes with TFIIH, CAK (Cdk7/Cyclin H/MAT1) and MMXD (MMS19-MIP18-XPD), and each of the complexes has distinct functions in DNA repair, transcription and cell cycle regulation (Ito *et al,* 2010). For instance, CAK cyclin dependent kinase is modulated by MAT1 therefore indispensable for cell cycle progression. MIP18 (MMS19-interacting protein 18 kDa) is part of the MMXD complex, which colocalized with mitotic spindle protein and involved in chromosome segregation.

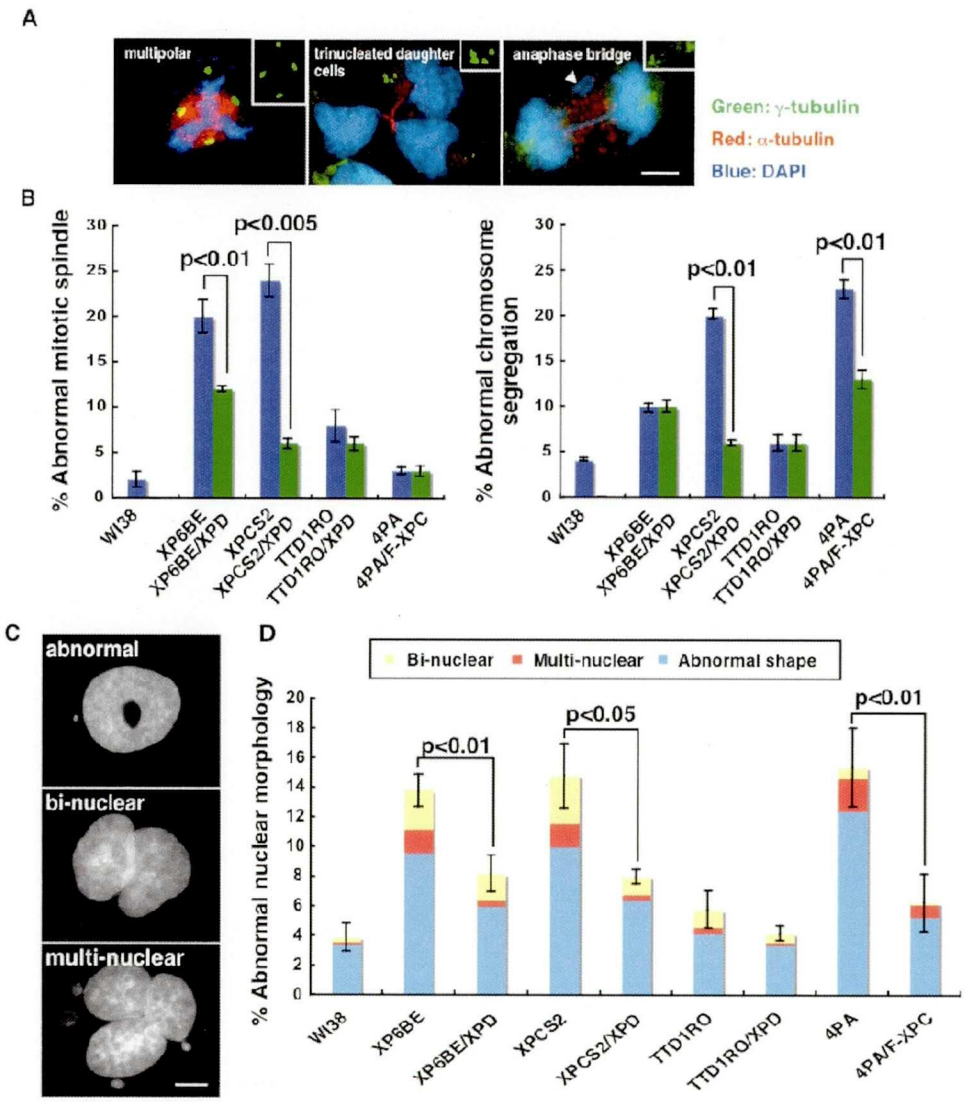

Figure 7. Phenotypic characterization of XPD, XP/CS, XP/TTD, XPC and wild type cells, WI38VA13 (A) Representation of abnormal mitosis cells with multipolar and abnormal chromosome segregation (B) Histograms show the average frequency of abnormal mitotic spindles and chromosome segregation. (N≥150 mitotic cells) (C) Representation of cells with abnormal nuclear morphology (D) Histograms show the average frequency of cells scored for abnormal nuclear morphology (N≥1500 cells). Error bars indicate SEM from three independent experiments. Scale bar, 10 μm.

Here, I showed that depletion of XPF led to aberrant centrosome and abnormal mitotic in normal cells. XP-F patient cells (XP2YOSV, XP42ROSV and XP51ROSV) exhibited phenotypes similar to siRNA mediated knockdown of XPF in normal fibroblast cells. WT-XPF is able to rescue the phenotypes in XP-F deficient cells, as well as NER and ICL repair functions. Alternatively, I employed other NER factors XPC and XPD deficient and proficient cell lines, respectively for characterization of mitotic and nuclear morphology cells profiles (Figure 7). Taken together, NER factors XPC, XPD and XPF were able to rescue its deficient cell lines with normal phenotypes similar to wild type cells. This suggests that NER factors XPC, XPD and XPF are indispensable for genome maintenance. It is possible that each of these NER factors regulate genome stability by using different mechanisms through the same molecular pathway, suggesting that the genotype-phenotype relationship for XPC, XPD and XPF govern genome stability by tethering mitotic chromosome segregation during cell division. Further understanding of how these factors coexist would provide much better clarity on the mechanism underlying DNA repair coupled with the cell cycle regulation in mammalian system.

References

Araki M, Masutani C, Takemura M, Uchida A, Sugasawa K, Kondoh J, Ohkuma Y, Hanaoka F (2001) Centrosome protein centrin 2/caltractin 1 is part of the xeroderma pigmentosum group C complex that initiates global genome nucleotide excision repair. *J Biol Chem* **22**:18665-72

Arora S, Kothandapani A, Tillison K, Kalman-Maltese V, Patrick SM (2010) Downregulation of XPF-ERCC1 enhances cisplatin efficacy in cancer cells. *DNA Repair (Amst)* **7**: 745-753

Bhagwat N, Olsen A, Wang AT, Hanada K, Stuckert P, Kanaar R, D'Andrea A, Niedernhofer LJ, McHugh PJ (2009) XPF-ERCC1 participates in the Fanconi anemia pathway of cross-link repair. *Mol Cell Biol* **29**: 6427-6437

Blangy A, Lane HA, d'Herin P, Harper M, Kress M, Nigg EA (1995) Phosphorylation by p34cdc2 regulates spindle association of human Eg5, a kinesin-related motor essential for bipolar spindle formation in vivo. *Cell* **83**: 1159-1169

DeBonis S, Simorre JP, Crevel I, Lebeau L, Skoufias DA, Blangy A, Ebel C, Gans P, Cross R, Hackney DD, Wade RH, Kozielski F (2003) Interaction of the mitotic inhibitor monastrol with human kinesin Eg5. *Biochemistry* **42**: 338-349

Ito S, Tan LJ, Andoh D, Narita T, Seki M, Hirano Y, Narita K, Kuraoka I, Hiraoka Y, Tanaka K (2010) MMXD, a TFIIH-Independent XPD-MMS19 Protein Complex Involved in Chromosome Segregation. *Mol Cell* **39**: 632-640

Jaspers NG, Raams A, Silengo MC, Wijgers N, Niedernhofer LJ, Robinson AR, Giglia-Mari G, Hoogstraten D, Kleijer WJ, Hoeijmakers JH, Vermeulen W (2007) First reported patient with human ERCC1 deficiency has cerebro-oculo-facio-skeletal syndrome with a mild defect in nucleotide excision repair and severe developmental failure. *Am J Hum Genet* **80**: 457-466

Kuraoka I, Kobertz WR, Ariza RR, Biggerstaff M, Essigmann JM, Wood RD (2000) Repair of an interstrand DNA cross-link initiated by ERCC1-XPF repair/recombination nuclease. *J Biol Chem* **275:** 26632-26636

Niedernhofer LJ, Garinis GA, Raams A, Lalai AS, Robinson AR, Appeldoorn E, Odijk H, Oostendorp R, Ahmad A, van Leeuwen W, Theil AF, Vermeulen W, van der Horst GT, Meinecke P, Kleijer WJ, Vijg J, Jaspers NG, Hoeijmakers JH (2006) A new progeroid syndrome reveals that genotoxic stress suppresses the somatotroph axis. *Nature* **444:** 1038-1043

Ogi T, Limsirichaikul S, Overmeer RM, Volker M, Takenaka K, Cloney R, Nakazawa Y, Niimi A, Miki Y, Jaspers NG, Mullenders LH, Yamashita S, Fousteri MI, Lehmann AR (2010) Three DNA polymerases, recruited by different mechanisms, carry out NER repair synthesis in human cells. *Mol Cell.* **37**: 714-27

Saijo T, Ishii G, Ochiai A, Yoh K, Goto K, Nagai K, Kato H, Nishiwaki Y, Saijo N (2006) Eg5 expression is closely correlated with the response of advanced non-small cell lung cancer to antimitotic agents combined with platinum chemotherapy. *Lung Cancer* **54:** 217-225

Sawin KE, Mitchison TJ (1995) Mutations in the kinesin-like protein Eg5 disrupting localization to the mitotic spindle. *Proc Natl Acad Sci U S A* **92:** 4289-4293

Schrader CE, Vardo J, Linehan E, Twarog MZ, Niedernhofer LJ, Hoeijmakers JH, Stavnezer J (2004) Deletion of the nucleotide excision repair gene Ercc1 reduces immunoglobulin class switching and alters mutations near switch recombination junctions. *J Exp Med* 3:321-30

Tian M, Shinkura R, Shinkura N, Alt FW (2004) Growth retardation, early death, and DNA repair defects in mice deficient for the nucleotide excision repair enzyme XPF. *Mol Cell Biol* **24:** 1200-1205

Weeda G, Donker I, de Wit J, Morreau H, Janssens R, Vissers CJ, Nigg A, van Steeg H, Bootsma D, Hoeijmakers JH (1997) Disruption of mouse ERCC1 results in a novel repair syndrome with growth failure, nuclear abnormalities and senescence. *Curr Biol* **7:** 427-439

Yagi T and Takebe H (1983) Establishment by SV40 transformation and characteristics of a cell line of xeroderma pigmentosum belonging to complementation group F. *Mutation Res* **112**: 59-66

Zhu XD, Niedernhofer L, Kuster B, Mann M, Hoeijmakers JH, de Lange T (2003) ERCC1/XPF removes the 3' overhang from uncapped telomeres and represses formation of telomeric DNA-containing double minute chromosomes. *Mol Cell* **12:** 1489-1498

Abstract

The XPF-ERCC1 complex is a structure-specific endonuclease involved in nucleotide excision repair (NER) and interstrand crosslink (ICL) repair. Patients with XPF mutations may suffer from two forms of xeroderma pigmentosum (XP): XP-F patients have a mild form of XP, while XFE patients display symptoms of accelerated aging. *Xpf* knockout mice display accelerated aging and die before weaning. These results suggest that the XPF-ERCC1 complex has additional functions besides NER and ICL repair and is essential for development and growth. In the present study we show that XPF interacts with kinesin Eg5 through the N-terminal region of XPF. Immunofluorescence staining revealed a dynamic colocalization between XPF and Eg5 during mitosis. XPF knockdown in cells led to an increase in the frequency of aberrant nuclear morphology and mitosis. In addition, the frequency of abnormal nuclei and of mitosis was increased in XPF and XFE cells. These results suggest that XPF plays a role in mitosis through its interaction with Eg5 and offer new insights into the pathogenesis of XPF and XFE.

Introduction

Nucleotide excision repair (NER) is a versatile and evolutionarily conserved repair pathway that removes a variety of DNA helix-distorting lesions such as ultraviolet (UV)-induced DNA damage and bulky DNA adducts. The importance of NER is highlighted by the existence of rare human disorders such as xeroderma pigmentosum (XP), Cockayne syndrome (CS) and trichothiodystrophy (TTD), which cause a wide range of clinical symptoms ranging from mild sun sensitivity to severe skin cancers, growth and developmental defects, neurological abnormalities and accelerated aging. Genetic complementation analysis revealed eight causative genes in XP (*XPA* through *XPG* and *XPV*), and two in CS (*CSA* and *CSB*). In rare cases mutations in the *XPB*, *XPD* and *XPG* genes cause features of CS combined with XP (XP/CS). Photosensitive TTD is associated with mutations in the *XPB*, *XPD* and *TTDA* genes (Friedberg *et al,* 2006).

The XPF protein forms a heterodimer with the *E*xcision *R*epair *C*ross-*C*omplementing rodent repair deficiency group *1* (ERCC1) protein, and the XPF-ERCC1 complex has a structure-specific endonuclease that cuts 5' of the DNA lesion in NER (Sijbers *et al,* 1996). Mutations in the *XPF* and *ERCC1* genes result in hypersensitivity to killing by UV and interstrand DNA crosslinking (ICL) agents, indicating that the XPF-ERCC1 complex plays essential roles in NER and ICL repair (Kuraoka *et al,* 2000). Patients with mutations in the *XPF* gene show mild photosensitivity and proneness to skin cancer but rarely show any neurological abnormalities. However, a case report has described the XFE (*XP*F-*E*RCC1) mutation in a patient displaying severe XP symptoms, growth retardation and accelerated aging

(Niedernhofer *et al*, 2006). Similarly the first patient with a mutation in the *ERCC1* gene displayed cerebro-oculo-facio-skeletal syndrome (COFS), including intrauterine growth retardation, simplified gyral pattern, cerebellar hypoplasia, failure to thrive and death at the age of 14 months (Jaspers *et al,* 2007). In addition, *Xpf-* or *Ercc1*-knockout (*Xpf-/-* or *Ercc1-/-)* mice suffer from accelerated aging and die before weaning (Tian *et al,* 2004). These results indicate that the XPF-ERCC1 complex plays important roles in multiple cellular functions such as NER, ICL repair, homologous recombination and telomere maintenance (Zhu *et al,* 2003). However, the causative relationship between these functions of XPF and the clinical features of XP-F and XFE has not been clarified.

In order to understand the functions of XPF we searched for XPF-binding proteins using affinity purification and mass spectrometry and identified a kinesin protein Eg5/Kif11/THRIP (Eg5). Eg5 is responsible for the formation and separation of the centrosome and spindle pole during pre- and post-mitosis (Sawin & Mitchison, 1995). Immunofluorescence staining revealed a dynamic colocalization between XPF and Eg5 during mitosis. Knockdown of XPF by siRNA resulted in an elevated frequency of abnormal nuclei and mitosis. In addition, cells from XP-F and XFE patients showed the same phenotypes as XPF-knockdown cells. Our results suggest that XPF plays a role in mitosis and is implicated in the pathogenesis of XP-F and XFE.

Results

XPF interacts with kinesin Eg5

In order to identify XPF-interacting proteins, FLAG-6xHis-tagged XPF cDNA was

stably expressed in HEK 293 cells. Nuclear extracts were subjected to a two-step affinity purification using anti-FLAG M2 agarose followed by nickel sepharose. The purified sample was separated by SDS-PAGE. Three bands (120, 110 and 37 kDa) were detected by silver staining (Figure 1A). Additionally, we observed a strong band at 120 kDa (p120), which was specific for the XPF-ERCC1 co-purified complex. The excised band was sent for MALDI-TOF/TOF mass spectrometry analysis (APRO Life Sciences Inst.) and identified as Eg5. The band at 110 kDa (p110) identified as XPF protein confirming the accuracy of mass spectrometry results (Table 1). Eg5 (HsEg5; NCBI accession number 13699824) was identified by the three tryptic-peptides SYLYPSTLVR, TTAATLMNAYSSR and LNLVDLAGSENIGR (Figure 1B).

To confirm the interaction between XPF and Eg5, the affinity-purified FLAG-6xHis-tagged XPF complex was subjected to western blotting using anti-XPF, anti-ERCC1, anti-Eg5 and anti-FLAG antibodies. As shown in Figure 2A, Eg5 was detected in the affinity-purified XPF complex. Subsequently, the FLAG-6xHis-tagged Eg5 cDNA was stably expressed in HEK 293 cells. The FLAG-6xHis-Eg5 complex was purified from nuclear extracts, and subjected to western blotting using the same antibodies. As shown in Figure 2A, XPF but not ERCC1 was co-immunoprecipitated with Eg5. Next, the ERCC1 cDNA tagged with FLAG-6xHis was stably expressed in HEK 293 cells, and the ERCC1-FLAG-6xHis complex was affinity purified. As shown in Figure 2B, XPF, but only a trace amount of Eg5, were coimmunoprecipitated with ERCC1. In order to confirm the interaction between XPF and Eg5, coimmunoprecipitations of the endogenous proteins were performed. Eg5 was

coimmunoprecipitated with both the anti-XPF antibody and the anti-ERCC1 antibody. However XPF, but not ERCC1, was coimmunoprecipitated with Eg5 using the anti-Eg5 antibody (Figure 2C).

In order to examine whether Eg5 binds directly to XPF-ERCC1, FLAG-XPF-ERCC1 and GST-Eg5 were expressed in *E. coli* and purified (Figure 2D). GST-Eg5 or GST was then mixed with FLAG-XPF-ERCC1. GST-pulldown and western blot analyses revealed that GST-Eg5 bound directly to FLAG-XPF, but not to ERCC1 (Figure 2D).

We studied the interaction of XPF and Eg5 during mitosis. Western blotting of HeLa cells synchronized by double thymidine block revealed that protein levels of XPF, ERCC1 and Eg5 were constant during the cell cycle (Figure 3A). XPF bound to Eg5 in nocodazole-treated mitotic cells as well as asynchronous cells (AS) (Figure 3B and C).

Eg5 interacts with the N-terminal region of the XPF protein

In order to determine the Eg5-binding region of XPF, four FLAG-tagged-XPF fragments (1-210, 1-320, 200-600, and 600-916 amino acid residues) and full-length XPF were stably expressed in HEK 293 cells, respectively (Figure 4A). The FLAG-XPF fragments were affinity purified from nuclear extracts. ERCC1 coimmunoprecipitated with full-length XPF and with the XPF C-terminal fragment (600-916 aa), but not with the N-terminal fragments. In contrast, Eg5 bound to the N-terminal fragments (1-210, 1-320 and 200-600 aa), but not to the C-terminal fragment (600-916 aa) of XPF, suggesting that Eg5 interacts with the N-terminal region of XPF

(Figure 4B).

Next, we investigated whether the interaction of XPF and Eg5 was affected by the XPF mutations derived from XP-F and XFE patients (Table 2, Figure 5A). The FLAG-tagged mutant XPF proteins were expressed in HEK 293 cells and affinity-purified from nuclear extracts. Immunoblots using anti-Eg5 antibody showed that all the mutant XPF proteins bound to Eg5 and ERCC1; however the V525STOP mutant did not bind to ERCC1 (Figure 5B).

Subcellular colocalization of XPF and Eg5

Since Eg5 functions in chromosome positioning, centrosome separation and establishment of a bipolar spindle during cell mitosis (Blangy *et al,* 1995), we investigated the subcellular localization of XPF during interphase and mitosis. GFP was fused in-frame with the N-terminus of XPF and stably expressed in HeLa cells. Prior to immunostaining, expression of GFP-XPF in HeLa cells was performed. GFP-tagged XPF in HeLa cells extract was subject to immunoprecipitation with anti-XPF antibody and analyzed by western blot analysis (Figure 6A). GFP-tagged XPF is specific to nuclear region during interphase while empty GFP vector in the cytoplasm and nuclear region (Figure 6D). On the other hand, GFP-XPF plasmid was transiently expressed in XP-F patient cells, XP2YOSV and subject to whole cell extract, cytoplasm and nuclear fractionation (Figure 6B and C). In addition, GFP-XPF/XP2YOSV cells were subjected to local UV irradiation and showed localization to the damage sites indicating GFP-XPF protein is functional (Figure 6E). The cells were synchronized at the G1/S phase using

a double thymidine block and released as described in Materials and Methods. The cells were then fixed and stained with anti-Eg5 (Figure 7A), anti-α-tubulin (Figure 7B) or anti-XPA (Figure 7C) antibody. As shown in Figure 7A, GFP-XPF was localized to the nucleus during interphase. In contrast, most Eg5 was localized to the cytoplasm, with some speckles detectable in the nucleus.

During the mitotic phase, Eg5 mainly colocalized with bipolar spindles. GFP-XPF was detected throughout the cells after breakdown of the nuclear membrane, and some of the GFP-XPF colocalized with Eg5 from metaphase to anaphase (Figure 7A). α-tubulin showed a staining pattern similar to that of Eg5, and GFP-XPF colocalized partially with α-tubulin (Figure 7B). However, XPA and FLAG-tagged ERCC1 did not colocalize with GFP-XPF or α-tubulin during mitosis (Figure 7C, Figure 8A and B).

Knockdown of XPF leads to abnormal nuclei and mitosis

We sought to assess the biological relevance of the interaction and colocalization of XPF and Eg5. Eg5 is required for proper bipolar spindle formation and cell cycle progression (Sawin & Mitchison, 1995). To determine whether XPF is also involved in mitotic pathways, the endogenous XPF was knocked down in the normal human cells WI38VA13 using XPF siRNA. Non-specific siRNA was used as a negative control. Whole cell extracts were prepared 24-120 hours after transfection of siRNA and subjected to western blotting (Figure 9A). A significant reduction in XPF protein levels was detected 72 hours after transfection of XPF siRNA compared to control siRNA

(Figure 9B and C). ERCC1 was also decreased in cells transfected with XPF siRNA, but Eg5 protein levels were the same in both XPF siRNA- and control siRNA-treated cells. XPF siRNA-treated cells showed hypersensitivity to killing by UV-irradiation and mitomycin C (MMC) treatment compared to control siRNA-treated cells (Figure 9D and E). FACS analysis showed normal cell cycle progression in siControl and siXPF-treated cells. However, the distribution of 6N DNA content, marked by a low peak was observed only in siXPF-treated cells (Figure 9F).

We examined whether knockdown of XPF led to abnormal nuclear morphology and mitosis in WI38VA13 cells. In order to distinguish siRNA-transfected cells from untransfected cells, siRNAs were labeled with Cy3 prior to transfection. Cells labeled with Cy3 were scored for abnormal nuclear morphology and mitosis. Groups of cells displaying abnormal nuclear morphology consisted of four subgroups: bi-, multi-, micro-nuclei and aberrant nuclear shapes (Figure 10A). Cells with abnormal nuclear morphology were four times more frequent upon XPF knockdown than in control cells (Figure 10C). Similarly, XPF knockdown led to abnormal centrosome (three or more γ-tubulin spots) ($p<0.03$, $n\geq1500$; Figure 10D). Cells in mitotic phase were quantified based on the staining patterns of α- and γ-tubulin in order to visualize mitotic spindles and centrosomes, respectively (Figure 10B). In cells with XPF knockdown, multipolar spindle and abnormal chromosome segregation occurred four and three times more often than in control cells ($p<0.03$ and $p<0.05$, $n\geq150$), respectively (Figure 10E). Consistent with these findings, FACS analysis showed that 6N DNA content was observed upon XPF knockdown (Figure 9F). Taken together,

these results suggest that XPF is involved in the formation of centrosome and/or mitotic spindles.

Abnormal nuclear morphology and mitosis in XP-F and XFE cells

In order to understand the relevance of XPF-mediated centrosome and/or mitotic spindle formation to the clinical features of XP-F and XFE patients (Table 2), we examined whether the frequency of abnormal nuclei and mitosis was increased in cells derived from XP-F and XFE patients. Figure 10A showed representative aberrant nuclei shapes and abnormal mitosis in XP-F cells (XP2YOSV). The frequency with which aberrant nuclei and abnormal centrosome and mitotic spindle/chromosome segregation were observed was increased by a factor of three to five in XP2YOSV cells compared to normal control human cells (WI38VA13) (Figure 10B). In order to verify that the increased frequency of abnormal nuclei and mitosis was due to the mutant XPF, XP2YOSV cells were transduced with lentivirus carrying FLAG-tagged wild-type (WT) or mutant XPF cDNAs derived from XFE and XP-F patients (R153P, R799W, I225M, and G513R) (Table 2). Lentivirus expressing V5-tagged LacZ was used as a negative control. The expression of ectopic FLAG-XPF was confirmed by western blotting (Figure 12A and B). Mutant XPF-expressing cells showed hypersensitivity to killing by UV-irradiation and exposure to MMC compared to cells expressing WT-XPF (Figure 12C and D). As shown in Figure 11B, the frequency of abnormal nuclei and mitosis in XP2YOSV cells expressing WT-XPF was similar to normal. However the frequency of abnormal nuclei and mitosis was only partially reduced upon expression of XPF

mutants R799W, I225M and G513R, which were derived from XP-F patients, and was not reduced upon expression of XPF mutant R153P, which was derived from an XFE progeroid patient (Figure 11D).

In order to confirm these findings, we examined the level of abnormal nuclei and mitosis in XFE cells (XP51ROSV) and XP-F cells (XP42ROSV). Consistent with the results in Figure 11B, the frequency of aberrant nuclei, abnormal centrosomes, and abnormal mitotic spindles/chromosome segregation was increased in XP51ROSV and XP42ROSV cells compared to normal control cells FS3SV (Figure 11C and D). The frequency of abnormal nuclei and mitosis was a little higher in XP51ROSV cells than in XP42ROSV cells (Figure 11D). We established WT-XPF cDNA-corrected isogenic cells: XP51ROSV/XPF and XP42ROSV/XPF (Figure 11C and D), and examined their level of abnormal nuclei and mitosis. The frequency of abnormal nuclei and mitosis was suppressed in the WT-XPF cDNA-corrected isogenic cells XP51ROSV/XPF and XP42ROSV/XPF (Figure 11D). Taken together, these results indicate that the abnormality in mitotic spindles/chromosome segregation of XP-F and XFE cells is due to the mutations in the *XPF* gene.

Discussion

Interaction between XPF and Eg5

In the present study, we showed that XPF interacts with kinesin Eg5 (Kif11/THRIP). Like many microtubule-related or cytoskeletal proteins, Eg5 is located mainly in the cytoplasm, whereas XPF is found in the nucleus. However, some Eg5 was detected in

the nucleus (Figure 1A and Figure 7A), and the interaction between XPF and Eg5 was detected in the mitotic and asynchronous cells (Figure 3B and C). However, knockdown of XPF did not affect the Eg5 protein level (Figure 3A). These results suggested that the XPF and Eg5 transiently interact during various phases of cell cycle including mitotic phase. The report that Eg5 exists in chromatin fraction as part of the histone H2A deubiquitinase complex and might act as a co-regulator of the H2A complex (Zhu *et al*, 2007) is consistent with our findings. The nucleolar protein B23 interacts with Eg5 (Wang *et al*, 2010). The kinesin protein Kif4 associates with poly (ADP-ribose) polymerase 1 (PARP1), a DNA repair and transcriptional regulator (Midorikawa *et al*, 2006).

Biochemical and structural studies of the XPF-ERCC1 complex indicate that homodimeric XPF is stable *in vitro*, but degrades quickly *in vivo* unless it interacts with ERCC1 as a heterodimer (Das *et al*, 2008). We showed that although Eg5 could coimmunoprecipitate with anti-XPF and anti-ERCC1 antibodies, respectively, ERCC1 did not coimmunoprecipitate with Eg5 using anti-Eg5 antibody (Figure 2A). When the FLAG-Eg5 was affinity purified from HEK 293 cells that had been transfected with FLAG-Eg5, XPF was detected in the FLAG-Eg5 complex but not ERCC1. In addition, only a trace amount of Eg5 was detected in the ERCC1-FLAG complex (Figure 2B), and GFP-XPF partially colocalized with Eg5 in the mitotic phase (Figure 7), while the ERCC1 did not colocalize with Eg5 (Figure 8). Taken together, these results suggest that XPF interacts with Eg5 in an ERCC1-independent manner and is stabilized by its interaction with Eg5.

As shown in Figure 4, Eg5 binds to the N-terminal fragments of XPF (1-210, 1-320 and 200-600 aa) of XPF. The N-terminal region of XPF contains the conserved region, the disrupted SF2-family helicase domains and the leucine zipper motifs (LZMs), while the C-terminal region contains the nuclease and the ERCC1-binding domains. Eg5 also has LZMs (Figure 4A and C). Proteins with LZMs can bind to DNA as either homodimers or heterodimers. LZMs are common among transcription factors important for growth regulation such as FOS, JUN and C/EB proteins (Schuermann *et al,* 1989). These findings suggest that XPF and Eg5 form a zipper through their respective LZMs.

The interaction of XPF and Eg5 is involved in mitosis

Our findings that XPF interacts with kinesin Eg5, which plays a role in the formation and separation of the centrosome and spindle pole during pre- and post-mitosis (Sawin & Mitchison, 1995), prompted us to investigate whether XPF is involved in mitosis. XPF partially colocalized with Eg5 in the mitotic cells, and knockdown of XPF resulted in increased centrosomes and abnormal chromosome segregation during the mitotic phase. XPF knockdown also caused abnormal nuclear shapes during the interphase. Knockdown of Eg5 resulted in cell cycle arrest with monopolar mitotic spindles (DeBonis *et al,* 2003), while knockdown of XPF did not affect cell cycle progression (Figure 9F). These results suggested that XPF plays a role in the regulation of Eg5-mediated formation and separation of centrosome and/or mitotic spindles in mitosis.

There have been an increasing number of studies focusing on the functions of DNA repair proteins in mitosis. XPB, XPD and FANCD2 proteins localize with the mitotic chromosomes, linking DNA damage and repair mechanisms to mitosis (Li *et al,* 2010; Naim & Rosselli, 2009; Weber *et al,* 2010) We previously reported that XPD forms a TFIIH-independent MMXD (MMS19, MIP18 and XPD) complex, and partially colocalizes with the mitotic spindle during mitosis. The siRNA-mediated knockdown of MMS19, MIP18 or XPD led to improper chromosome segregation and the accumulation of nuclei with abnormal shapes, respectively. The same phenotypes were observed in XP-D and XP-D/CS cells, but not in XP-D/TTD cells. These results indicated that XPD exists as one of the core subunits of the MMXD complex and is engaged in chromosome segregation in addition to NER and transcription, and suggested that deficiency in MMXD could contribute to the pathogenesis of XP-D and XP-D/CS (Ito *et al,* 2010).

Clinical implication of abnormal mitosis in XP-F and XFE cells

The accelerated aging symptoms observed in XFE and the ERCC1/COFS patients (Jaspers *et al,* 2007; Niedernhofer *et al,* 2006) and the *Xpf*-/- and the *Ercc1*-/- mice (Tian *et al,* 2004; Niedernhofer *et al,* 2006) are not solely due to a defect in NER, because XP-A patients and *Xpa*-/- mice with almost complete defect in NER do not show such symptoms. XPF-ERCC1 has essential functions for development and viability, and patients with homozygous nonsense or frame-shift mutations in the *XPF* or *ERCC1* genes have not been found.

It has been reported that *Ercc1-/-* mice showed a decreased level of insulin-like growth factor 1 (IGF-1) (Niedernhofer *et al*, 2006). The insulin/IGF-1 is inhibited in response to DNA damage in order to inhibit cell growth and to minimize the formation of DNA damage. Although inactivation of the insulin/IGF-1 pathway promotes longevity, the persistent and rapid accumulation of DNA damage due to the XPF/ERCC1-deficiency could induce accelerated aging. These observations have suggested that somatotropic attenuation represents a response to accumulating DNA damage. It has been suggested that ICL and oxidative DNA damage could be the primary DNA lesions responsible for the accelerated aging phenotype of *Ercc1-/-* and *Xpf-/-* mice (Wijnhoven *et al,* 2007). In the present study, we showed that the frequency of aberrant nuclei, and abnormal centrosomes and mitotic spindles was increased in XP-F and XFE cells. In addition, the XP2YOSV (XP-F) cells expressing mutant XPF derived from other XP-F patients (R799W, I225M and G513R) showed some recovery from abnormal mitosis, while the XP2YOSV cells expressing the mutant XPF derived from XFE patient (R153P) showed no or less recovery (Figure 11B). There was a correlation between the severity of the clinical features and the level of abnormal mitosis in XP-F and XFE patients, suggesting that at least part of the accelerated aging symptoms in the XFE patient is due a defect in mitosis. Consistent with our results, the *Ercc1-/-* and the *Xpf-/-* mice showed liver cells with enlarged and abnormal nuclei shapes (Weeda *et al,* 1997). Recent studies have demonstrated that *Eg5-/-* mice suffer from embryonic death before the implantation stage (Chauvière *et al,* 2008), implying that Eg5 is essential for early development. In addition, defects in kinesin and

microtubules are associated with neurological and premature aging diseases that resemble the features in the XFE patient and the *Ercc1-/-* and the *Xpf-/-* mice (Ferhat *et al,* 1998; Wijnhoven *et al,* 2007). However, we cannot exclude the possibility that the abnormal nuclei and mitosis observed in the XPF-knockdown cells and in the XP-F and XFE cells might be caused by defects in ICL repair, homologous recombination and/or telomere maintenance, since such defects might impair DNA replication and transcription and prevent proper chromatin dynamics resulting in the missegregation of chromosomes during mitosis (Kuraoka *et al,* 2000; Sijbers *et al,* 1996; Zhu *et al,* 2003). It is important to further elucidate the role of XPF and that of its interaction with Eg5 in mitosis and to understand how they relate to the pathogenesis of XP-F and XFE.

On the other hand, knocking down Eg5 resulted in expected cell cycle arrest in monopolar spindles (Blangy *et al,* 1995). Conversely, depletion of XPF did not affect cell cycle progression or mitotic arrest (Figure 9F). To verify these results, we performed single and double knockdown of XPF. Western blots showed a significant reduction in the XPF protein whereas Eg5 protein levels remained unaffected in both XPF and control siRNA treated cells (Figure 9B). This suggests that XPF and Eg5 are independent of each other and indispensable for maintaining normal cellular function in a cell network. Despite the fact both XPF and Eg5 have opposite profiles in term of function and cellular compartmentalization, they are mutually essential for early embryo development and cell regulation, and can act as predicative biomarker for cancer. Taken together, our results demonstrate that XPF has cell cycle related subcellular localization, suggesting a role in the coupling of the cell cycle and genome stability. Based on the

phenotypic characterization of XPF siRNA and XP-F patient cells, XPF is essential for growth and normal development in the eukaryotic system. Further studies are necessary to better understand and uncover the presence of a genetic link for the XPF-Eg5 complex by which a new cancer marker or cancer drug will arise.

Materials and Methods

Cell cultures

Cell lines used were listed in Table 2 and described in Materials and Methods of Supplementary Information. Cells were maintained in Dulbecco's modified Eagle's medium (Nissui) supplemented with 10% fetal bovine serum, 2 mM L-glutamine, 100 U/ml penicillin, and 100 μg/ml streptomycin in a humidified incubator at 37°C supplied with 5% CO_2. Transfection of plasmids was performed using Effectene (Qiagen) or Lipofectamine 2000 (Invitrogen) according to the manufacturer's recommendations. Transfection using the ON-Targetplus SMARTpool XPF siRNA (Thermo Fisher Scientific) or a non-specific siRNA was performed using Lipofectamine RNAimax (Invitrogen). For labeling of siRNAs with Cy3, the Silencer siRNA labeling kit (Ambion) was used.

Cell lines

The cell lines used in this study were HEK 293 (Flp-In-293, Invitrogen) SV40 immortalized human fibroblasts; WI38 or WI38VA13 (normal), FS3SV (normal), XP2YOS or XP2YOSV (XP-F), and XP12ROSV (XP-A). The hTERT-immortalized XP51RO (XFE) and XP42RO (XP-F) cells, provided by L. Niedernhofer, were further transformed by the transfection with plasmid containing SV40-large T antigen. The patients' cells were transduced with lentiviral vector, pLenti6 (Invitrogen) containing the wild type XPF (XP2YOSV/XPF, XP51ROSV/XPF, XP42ROSV/XPF), and the mutant XPF (XP2YOSV/R153P, XP2YOSV/R799W, XP2YOSV/I225M,

XP2YOSV/G513R), respectively, and pLenti6-V5-LacZ as a vector control.

Plasmids and pLenti viral expression systems

XPF and Eg5 cDNAs were isolated by RT-PCR from HeLa cell mRNA. cDNAs for four truncated XPF, corresponding to 1-210, 1-320, 200-600 and 600-916 amino acid residues, were amplified by PCR. XPF cDNA with point mutation were generated using a QuikChange site-directed mutagenesis kit (Strategene). The isolated PCR products were cloned into pcDNA5/FRT/V5-His-TOPO TA (Invitrogen) with FLAG and 6xHis tags at the N-terminal. Wild type or mutant XPF cDNA was inserted in pLenti6 viral expression vector (Invitrogen). Viral production and transduction were performed according to the manufacturer's protocol. DNA sequencing excluded additional mutations introduced elsewhere in the cDNAs.

Protein purification and analysis

Nuclear extracts were prepared as described previously (Vlcek *et al,* 1999). FLAG-6xHis-tagged proteins were affinity-purified from nuclear extracts using anti-FLAG M2 agarose (Sigma) and Nickel Sepharose (GE Healthcare). Bound proteins were eluted with 0.2 mg/ml FLAG peptide (Sigma) in NETN buffer (50 mM Tris-HCl [pH 7.5], 150 mM NaCl, 1 mM EDTA, 1% NP-40, 1 mM DTT, and 0.25 mM PMSF-phenylmethylsulfonyl fluoride) and 200 mM imidazole in NTN buffer (50 mM [pH 7.5], 150 mM NaCl,, 1% NP-40, 1 mM DTT, and 0.25 mM PMSF) at each step. HeLa whole cell extracts were subjected to immunoprecipitation using indicated

antibodies coupled with protein G Sepharose (GE Healthcare). Proteins were denatured at 95°C in SDS-lysis buffer and subjected to 10% SDS-PAGE, followed by silver staining (WAKO), Coomassie brilliant blue staining (Nacalai Tesque) or Western blotting (ECL plus detection kit, GE Healthcare).

Protein purification for bacterial work

pCOLADuet-FLAG-6xHis-XPF/ERCC1 and pGEX-GST-FLAG-6xHis-Eg5 were introduced into *E. coli* strain Rosetta 2 (Invitrogen) and BL21 (DE3), respectively. *E. coli* was cultured, and subjected to cell lysis by sonification in NETN buffer (50 mM Tris-HCL, pH7.8, 150 mM NaCl, 1 mM EDTA, 1% Nonidet p-40, 10 mM 2-mercaptoethanol, 0.5 mM PMSF and complete protease inhibitor, Roche). Proteins were affinity-purified from the cell lysates as previously described here.

Immunofluorescence

Cells were fixed in 4% paraformaldehyde for 15 min and permeabilized with 0.2% Triton X-100 in PBS for 5 min. For cytoskeleton proteins, cells were dehydrated with methanol chilled at -20°C. Cells were incubated with 1% BSA in PBS, and then with primary and secondary antibodies for 60 min, each followed by three 5 min washes after the incubations with antibodies. Coverslips were mounted in Vectashield with DAPI (Vector Laboratories). Cells were imaged using a 60x 1.49 NA lens on a Nikon Ti Eclipse inverted microscope and deconvolved using NIS-Elements Advanced Research software.

Antibodies

Rabbit anti-Eg5 polyclonal antibody was raised against synthetic peptides (amino acids 1-14 [MASQPNSSAKKKEEC], 964-976 [CSENNKEETIPDV] and 1013-1027 [CQHKKSHGKDKENRGI] of Eg5). Commercially available antibodies used were anti-Eg5 (10C7; BioLegend, used at the dilution of 1:1000), anti-XPF (C51; NeoMarkers, 1:500), anti-ERCC1 (3HII; Serotec, 1:1000), anti-DDDDK-Tag (MBL, 1:1000), cyclin B1 (H-433; SantaCruz, 1: 1500), α-tubulin (YOL1/34; Abcam, 1:2000, DM1A; Sigma, 1:1000) and γ-tubulin (T6557; Sigma, 1:2000). Secondary antibodies were peroxidase-conjugated anti-mouse and anti-rabbit IgG antibodies (GE Healthcare, 1:5000), and to Alexa Fluor 488- and Alexa Fluor 568- conjugated (Molecular Probes, 1:1500).

Cell-cycle synchronization

About 2 x 10^6 HeLa cells expressing GFP-XPF were seeded and incubated in 10% FBS/DMEM containing 2 mM thymidine for 18 hrs. After washing with PBS, cells were incubated for 9 hrs in 10% FBS/DMEM, and incubated with 10% FBS/DMEM containing 2 mM thymidine for another 17 hrs. The cells synchronized at G1/S were then released from the thymidine block, and collected at every 2 hrs intervene to prepare the samples for flow cytometer analysis (FACSCalibur, BD Biosciences) and protein analysis.

Clonogenic Survival Assay

About 2000 – 4000 cells were seeded 6-12 hrs prior to exposure with UV-irradiation or MMC-treatment (Wako). Cells were incubated for 2 weeks, fixed with 10% formalin in PBS, and stained with 0.1% (w/v) Crystal violet. Survived colony with about more than 50 cells was counted.

Local UV irradiation

Prior to UV irradiation, HeLa cells stably expressing GFP-tagged XPF were seeded on coverslip in a 35 mm dish. Cells were locally irradiated with 100 Jm^{-2} of UV-C through an Isopore polycarbonate membrane filter with a pore size of 5 μm (Milipore) and incubated for 20 min in humidified incubator at 37°C supplied with 5% CO_2. Cells were subjected to immunostaining and microscopy as mentioned somewhere in Materials and Methods.

Statistical Analysis

For quantifications of abnormal nuclear shape and mitosis, at least 1500 interphase cells and 150 mitotic cells were counted from three independent experiments. Student t-tests were used for statistical analyses ($p<0.05$ defined statistically significant).

References

Arora S, Kothandapani A, Tillison K, Kalman-Maltese V, Patrick SM (2010) Downregulation of XPF-ERCC1 enhances cisplatin efficacy in cancer cells. *DNA Repair (Amst)* **7:** 745-753

Blangy A, Lane HA, d'Herin P, Harper M, Kress M, Nigg EA (1995) Phosphorylation by p34cdc2 regulates spindle association of human Eg5, a kinesin-related motor essential for bipolar spindle formation in vivo. *Cell* **83:** 1159-1169

Chauvière M, Kress C, Kress M (2008) Disruption of the mitotic kinesin Eg5 gene (Knsl1) results in early embryonic lethality. *Biochem Biophys Res Commun* **372:** 513-519

Das D, Tripsianes K, Jaspers NG, Hoeijmakers JH, Kaptein R, Boelens R, Folkers G (2008) The HhH domain of the human DNA repair protein XPF forms stable homodimers. *Proteins* **70:** 1551-1563

DeBonis S, Simorre JP, Crevel I, Lebeau L, Skoufias DA, Blangy A, Ebel C, Gans P, Cross R, Hackney DD, Wade RH, Kozielski F (2003) Interaction of the mitotic inhibitor monastrol with human kinesin Eg5. *Biochemistry* **42:** 338-349

DeBonis S, Simorre J, Crevel I, Lebeau L, Skoufias DA, Blangy A, Ebel C, Gans P, Cross R, Hackney DD, Wade RH, Kozielski F (2003) Interaction of the mitotic inhibitor monastrol with human kinesin Eg5. *Biochemistry* **42:** 338-349

Ferhat L, Cook C, Chauviere M, Harper M, Kress M, Lyons GE, Baas P (1998) Expression of the mitotic motor protein Eg5 in postmitotic neurons: implications for neuronal development. *J Neurosci* **18:** 7822-7835

Friedberg E, Aguilera A, Gellert M, Hanawalt PC, Hays JB, Lehmann AR, Lindahl T, Lowndes N, Sarasin A, Wood R (2006) DNA repair: from molecular mechanism to human disease. *DNA Repair (Amst)* **5:** 986-996

Ito S, Tan LJ, Andoh D, Narita T, Seki M, Hirano Y, Narita K, Kuraoka I, Hiraoka Y, Tanaka K (2010) MMXD, a TFIIH-Independent XPD-MMS19 Protein Complex Involved in Chromosome Segregation. *Mol Cell* **39:** 632-640

Jaspers NG, Raams A, Silengo MC, Wijgers N, Niedernhofer LJ, Robinson AR, Giglia-Mari G, Hoogstraten D, Kleijer WJ, Hoeijmakers JH, Vermeulen W (2007) First reported patient with human ERCC1 deficiency has cerebro-oculo-facio-skeletal syndrome with a mild defect in nucleotide excision repair and severe developmental failure. *Am J Hum Genet* **80:** 457-466

Kuraoka I, Kobertz W, Ariza RR, Biggerstaff M, Essigmann JM, Wood R (2000) Repair of an interstrand DNA cross-link initiated by ERCC1-XPF repair/recombination nuclease. *J Biol Chem* **275:** 26632-26636

Li X, Urwyler O, Suter B (2010) Drosophila Xpd regulates Cdk7 localization, mitotic kinase activity, spindle dynamics, and chromosome segregation. *PLoS Genet* **6:** e1000876

Midorikawa R, Takei Y, Hirokawa N (2006) KIF4 motor regulates activity-dependent neuronal survival by suppressing PARP-1 enzymatic activity. *Cell* **125:** 371-383

Naim V, Rosselli F (2009) The FANC pathway and BLM collaborate during mitosis to prevent micro-nucleation and chromosome abnormalities. *Nat Cell Biol* **11:** 761-768

Niedernhofer LJ, Garinis GA, Raams A, Lalai AS, Robinson AR, Appeldoorn E, Odijk H, Oostendorp R, Ahmad A, van Leeuwen W, Theil AF, Vermeulen W, van der Horst GT, Meinecke P, Kleijer WJ, Vijg J, Jaspers NG, Hoeijmakers JH (2006) A new progeroid syndrome reveals that genotoxic stress suppresses the somatotroph axis. *Nature* **444:** 1038-1043

Olaussen KA, Dunant A, Fouret P, Brambilla E, André F, Haddad V, Taranchon E, Filipits M, Pirker R, Popper HH, Stahel R, Sabatier L, Pignon JP, Tursz T, Le Chevalier

T, Soria JC (2006) DNA repair by ERCC1 in non-small-cell lung cancer and cisplatin-based adjuvant chemotherapy. *N Engl J Med* **355:** 983-991

Saijo T, Ishii G, Ochiai A, Yoh K, Goto K, Nagai K, Kato H, Nishiwaki Y, Saijo N (2006) Eg5 expression is closely correlated with the response of advanced non-small cell lung cancer to antimitotic agents combined with platinum chemotherapy. *Lung Cancer* **54:** 217-225

Sawin KE, Mitchison TJ (1995) Mutations in the kinesin-like protein Eg5 disrupting localization to the mitotic spindle. *Proc Natl Acad Sci U S A* **92:** 4289-4293

Schuermann M, Neuberg M, Hunter JB, Jenuwein T, Ryseck RP, Bravo R, Müller R (1989) The leucine repeat motif in Fos protein mediates complex formation with Jun/AP-1 and is required for transformation. *Cell* **56:** 507-516

Sijbers AM, de Laat WL, Ariza RR, Biggerstaff M, Wei YF, Moggs JG, Carter KC, Shell BK, Evans E, de Jong MC, Rademakers S, de Rooij J, Jaspers NG, Hoeijmakers JH, Wood RD (1996) Xeroderma pigmentosum group F caused by a defect in a structure-specific DNA repair endonuclease. *Cell* **86:** 811-822

Tian M, Shinkura R, Shinkura N, Alt F (2004) Growth retardation, early death, and DNA repair defects in mice deficient for the nucleotide excision repair enzyme XPF. *Mol Cell Biol* **24:** 1200-1205

Vlcek S, Just H, Dechat T, Foisner R (1999) Functional diversity of LAP2alpha and LAP2beta in postmitotic chromosome association is caused by an alpha-specific nuclear targeting domain. *EMBO J* **18:** 6370-6384

Wang G, Gao X, Huang Y, Yao Z, Shi Q, Wu M (2010) Nucleophosmin/B23 inhibits Eg5-mediated microtubule depolymerization by inactivating its ATPase activity. *J Biol Chem* **285:** 19060-19067

Weber A, Chung HJ, Springer E, Heitzmann D, Warth R (2010) The TFIIH subunit p89 (XPB) localizes to the centrosome during mitosis. *Cell Oncol* **32:** 121-130

Weeda G, Donker I, de Wit J, Morreau H, Janssens R, Vissers C J, Nigg A, van Steeg H, Bootsma D, Hoeijmakers J (1997) Disruption of mouse ERCC1 results in a novel repair syndrome with growth failure, nuclear abnormalities and senescence. *Curr Biol* **7:** 427-439

Wijnhoven S, Hoogervorst EM, de Waard H, van der Horst GT, van Steeg H (2007) Tissue specific mutagenic and carcinogenic responses in NER defective mouse models. *Mutation Research* **614:** 77-94

Zhu X, Niedernhofer L, Kuster B, Mann M, Hoeijmakers JH, de Lange T (2003) ERCC1/XPF removes the 3' overhang from uncapped telomeres and represses formation of telomeric DNA-containing double minute chromosomes. *Mol Cell* **12:** 1489-1498.

Figure Legends

Figure 1. XPF interacts with Eg5

(A) XPF was affinity-purified with anti-FLAG antibody from nuclear extracts of HEK 293 cells expressing FLAG-6xHis-XPF. The purified samples were resolved by SDS-PAGE and proteins were visualized by silver staining. Polypeptides identified by mass spectrometry are shown. A sample from HEK 293 cells was used as a mock negative control. Mass spectrometry identified polypeptides in the sample are shown. HEK 293 cells as a mock for negative control. (B) MALDI peptide mass fingerprint analysis of the tryptic digested 120 kDa band identified three proteins, TTAATLMNAYSSR, LNLVDLAGSENIGR AND SYLYPSTLVR, which are all conserved proteins in Eg5. Schematic overview of human Eg5 indicating three distinct domains: motor (light gray), stalk (white) and tail (dark gray). Phosphorylation sites are indicated with a black bar. MALDI-TOF peptide mass fingerprinting analysis of the 120 kDa band identified three peptides (TTAATLMNAYSSR, LNLVDLAGSENIGR and SYLYPSTLVR) which were part of the conserved domains of Eg5.

Table 1. Summary of MS-Fit search results for Eg5 protein Band p120 was identified as Kinesin family member 11 (Kif11)/Eg5 while band p110 as ERCC4/XPF. Band name, comparison between experimental and theoretical molecular weight (kDa), protein name and NCBI accession number as shown in the table.

Figure 2. Analysis of the interaction between XPF and Eg5

(A) Eg5 and XPF were affinity-purified with anti-FLAG antibody from nuclear extracts of HEK 293 expressing FLAG-Eg5 and FLAG-XPF, respectively. The affinity-purified XPF and Eg5 samples were analyzed by immunoblotting using the indicated antibodies. (B) ERCC1 was affinity-purified from nuclear extracts of HEK 293 cells expressing ERCC1-FLAG-6xHis. The affinity-purified ERCC1 sample was subjected to immnoblotting using the antibodies indicated. (C) Whole cell extracts from HeLa cells were immunoprecipitated with anti-XPF, -Eg5 or -ERCC1 antibody. The immunoprecipitated proteins were subjected to western blotting with the antibodies indicated. (D) *In vitro* binding assay using purified proteins. GST-Eg5 and FLAG-6xHis-ERCC1-XPF were expressed in *E. coli* and purified. Coomassie brilliant blue staining of the sample resolved by SDS-PAGE is shown (left). FLAG-6xHis-ERCC1-XPF was incubated with GST or GST-Eg5 after which the GST-pull down assay was performed. Western blots are shown (right).

Figure 3. Expression profiles of XPF and Eg5 during cell cycle

(A) HeLa cells were synchronized at the G1/S boundary using the double thymidine block method. Cells were harvested at 2 hr intervals after release from thymidine block and subjected to western blot analysis. FACS analysis was performed on the same cell samples to verify cell cycle distributions at each time point after release from thymidine block. (B) HeLa cells were treated with 0.1 μg/ml Nocodazole for 18 hrs to induce mitotic block (M). Whole cell lysates from mitotic (M) and asynchronized (AS) cells

were subjected to immunoprecipitation with anti-Eg5 antibody. Mouse IgG was used as a negative control. (C) Whole cell lysates from Nocodazole-treated HeLa cells were subjected to immunoprecipitation with anti-XPF, -ERCC1 or -Eg5 antibodies, respectively. Western blotting in (A) to (C) was performed with the antibodies indicated.

Figure 4. Eg5 binds to the N-terminal region of XPF

(A) Schematic overview of full-length (FL) and truncated XPF. Functional domains in XPF are depicted. (B) FLAG-tagged full-length or truncated XPF was expressed in HEK 293 cells and immunoprecipitated with anti-FLAG beads. Western blots were probed with the antibodies indicated. (C) Amino acid sequence alignments of leucine zipper motifs found in XPF and Eg5. The leucine zipper motif is defined as the consensus sequence L-x(6)-L-x(6)-L-x(6)-L. Note that the dark shades indicate highly conserved residues whereas gray shades represent less conserved residues.

Figure 5. Eg5 binds to XPF mutants mimicking XP-F patients

(A) Arrows indicate the location of mutations in XPF. Functional domains in XPF are depicted in Figure 4A. (B) XPF proteins were affinity-purified with anti-FLAG beads from nuclear extracts of HEK 293 cells expressing WT or mutant FLAG-6xHis-XPF. The proteins were eluted, resolved by SDS-PAGE and analyzed by western blotting analysis using the antibodies indicated.

Table 2. Clinical features and mutations of XP-F patients

All XPF mutations, cell line name, patient age, clinical features and clinical severity were as shown.

Figure 6. Stable expression of GFP-XPF in HeLa cells and transient expression of GFP-XPF in XP2YOSV cells

(A) Whole cell extracts from HeLa cells stably expressing GFP-tagged XPF were subjected to immunoprecipitation with anti-XPF antibody and mouse IgG as negative control. Samples were subjected to SDS-PAGE and western blot analysis. GFP-tagged XPF was transiently expressed in XP2YOSV cells and subjected to cellular fractionation to obtain whole cell extract (B), cytoplasm and nuclear fractions (C). The fractionated samples were subjected to SDS-PAGE and western blot analysis. An asterisk represents GFP protein in an empty vector as negative control. (A-C) Antibodies used were as indicated. (D) Localization of empty GFP vector and GFP-tagged XPF stably expressed in HeLa cells. (E) GFP-tagged XPF protein localized to the damaged DNA sites after cells were subjected local UV irradiation

Figure 7. Colocalization of GFP-XPF and Eg5 during mitotic phase in HeLa cells

(A) HeLa cells expressing GFP-XPF were synchronized at the G1/S boundary by the double thymidine block method and released to allow the cells to progress to S phase. At each point, cells were fixed and visualized by fluorescent immunostaining using anti-Eg5 antibody (red). GFP-XPF and DNA are shown in green and blue, respectively.

Anti-α-tubulin and anti-XPA antibodies were used for immunostaining in (B) and (C), respectively. Scale bar, 10 μm.

Figure 8. Colocalization of FLAG-XPF and Eg5 during mitotic phase in HEK 293 cells

HEK 293 cells stably expressing FLAG-XPF or ERCC1-FLAG were subjected to fluorescence immunostaining with anti-FLAG (green) and anti-Eg5 (red) (A) or anti-α-tubulin (red) (B). DNA was stained with DAPI (blue).

Figure 9. Protein levels, sensitivity to UV or mitomycin C (MMC) and cell cycle profile of XPF-knockdown cells

(A) Normal human WI38VA13 cells were transfected with control siRNA or XPF siRNA (Dharmacon). The cells were harvested every 24 hrs post-transfection until 120 hrs. Western blot analysis of whole cell lysates was performed using anti-XPF and anti-ERCC1 antibodies. β-tubulin was used as a loading control. For the clonogenic survival assay, siControl- or siXPF-transfected cells (72 hrs after transfection) were seeded and exposed to UV light (B) or MMC (C) at the concentrations indicated. Each point represents the average ± standard error (SE) of the mean from three independent experiments. (D) SiRNA-transfected cells (72 hrs after transfection) were analyzed by flow cytometry to determine cell cycle profiles.

Figure 10. Knockdown of XPF induces nuclear abnormality and mitotic aberrations

(A) Control or XPF siRNA was transfected into the normal human cells WI38VA13. The cells were collected at 72 hrs post-transfection. The whole cell extracts were subjected to western blotting using the antibodies indicated. (B) Quantitative RT-PCR was performed to detect XPF mRNA in control or XPF siRNA-transfected cells. Bars indicate SD obtained from three independent experiments. (C) Representative immunofluorescence analysis of control siRNA-transfected (siControl) and XPF siRNA-transfected (siXPF) cells. Abnormal nuclei include micro-, bi-, multi-nuclei and aberrant shapes in interphase. The centrosome region is highlighted in the inset of each image. White arrowhead indicates micro-nuclei. (D) Representative immunofluorescence of normal mitotic bipolar cells (siControl) and abnormal mitotic cells (siXPF). Mitotic aberrations include multi-polar centrosome and abnormal chromosome segregation (missegregation, tri-nucleated telophase and anaphase bridge). Images of siControl and siXPF cells stained with anti-α-tubulin (mitotic chromosomes are highlighted in the inset of each image) and anti-γ-tubulin (centrosomes are highlighted in the inset of each image). Scale bar, 10 μm. siRNA was labeled with Cy3 (red) and transfected into the WI38VA13 normal human cells. Cells were fixed and stained with anti-α-tubulin and -γ-tubulin (green), respectively. DNA was stained with DAPI (blue). For quantification, interphase cells (n≥1500) were scored for abnormal nuclear morphology (E) and centrosome number (F). (G) M phase cells (n≥500) were scored for multi-polar and abnormal chromosomes. The data were obtained from three

independent experiments. Histograms show average percentage ± standard deviation. The difference between siXPF and siControl cells was statistically significant. Significant p values are indicated: *($p<0.03$) and **($p<0.05$).

Figure 11. Nuclear abnormality and mitotic aberration in XP-F and XFE cells

(A) XP-F cells (XP2YOSV) were fixed and stained with anti-α-tubulin (red), -γ-tubulin (green) and DAPI (blue). Images represent abnormal nuclear shapes such as bi-, multi- and micro-nuclei in interphase cells, and abnormal mitotic cells that were divided into two subgroups: multi-polar, and abnormal chromosome segregation (lagging chromosomes). The inset in each image shows a view highlighted on centrosomes. White arrowheads indicate micro-nuclei. (B) Histograms show abnormal nuclear morphology, centrosome number and multi-polar and abnormal chromosomes in XP2YOSV cells and in XP2YOSV cells expressing wild-type and various mutant XPF cDNAs, respectively. Quantification was performed as described in Figure 9. Significant p values are indicated. * ($p<0.01$), **($p<0.03$) and ***($p<0.05$). (C) A normal fibroblast, FS3SV, and XP-F cells were subjected to immunofluorescence staining with anti-α-tubulin (red) and -γ-tubulin antibodies. Patient cell lines were XP51ROSV and XP42ROSV, which carry the homozygous mutations R153P and R799W, respectively. DNA was stained with DAPI (blue). Images represent normal human cells FS3SV (left), XP51ROSV (middle) and XP42ROSV (right). Insets in each image show the view highlighted on centrosomes. Scale bar, 10 μm. (D) Both XP51ROSV and XP42ROSV were transduced with pLenti6-WT-XPF. Cells were

scored for abnormal nuclear morphology and mitotic aberrations as described in Figure 10. Significant p values are indicated. * ($p<0.01$), **($p<0.03$) and ***($p<0.05$).

Figure 12. Expression of WT or mutant XPF in XP2YOSV cells and clonogenic survival after UV irradiation or MMC treatment

(A) Expression of WT and mutant XPF in XP2YOSV cells was checked by western blot analysis using antibodies as indicated. Lane 1, WI38VA13; lane 2, V5-LacZ; lane 3, WT-XPF; lane 4, R153P; lane 5, R799W; lane 6, G513R; lane 7, I225M. (B) Expression of WT XPF in XP51ROSV and XP42ROSV cells was checked by western blot analysis. Lane 1, FS3SV; lane 2, XP51ROSV/V5-LacZ; lane 3, XP42ROSV/V5-LacZ; lane 4, XP51ROSV/WT-XPF; lane 5, XP42ROSV/WT-XPF. (C and D) Survival of XP2YOSV cells expressing WT-XPF, mutant XPF or V5-LacZ upon exposure to UV light or MMC. WI38VA13 cells are normal human cells while XP12ROSV cells are XP-A cells. Each point represents the average ± standard error (SE) of the mean from three independent experiments. (E and F) Survival of the following cells upon exposure to UV light or MMC: FS3SV (normal), XP42ROSV (XP-F), XP51ROSV (XFE), WT-XPF-corrected XP42ROSV (XP42ROSV/XPF) and WT-XPF-corrected XP51ROSV (XP51ROSV/XPF) cells. Each point represents the average ± standard error (SE) of the mean from three independent experiments.

Figure 1

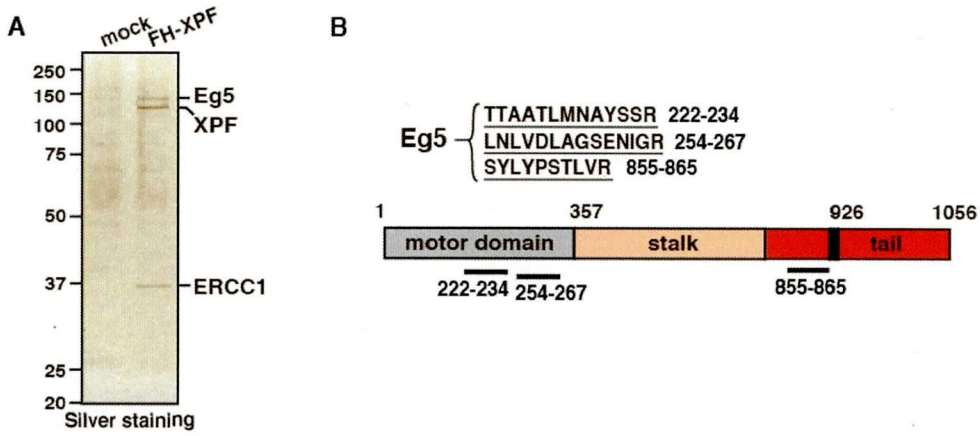

Table 1. Summary of MS-Fit search results for Eg5 protein

Band name	Experimental/ Theoretical (kDa)	Protein Name	NCBI Accession No.
p120	120 / 119.16	Kinesin family member 11/Eg5	13699824
p110	110 / 103.29	ERCC4/XPF	2842712

Figure 2

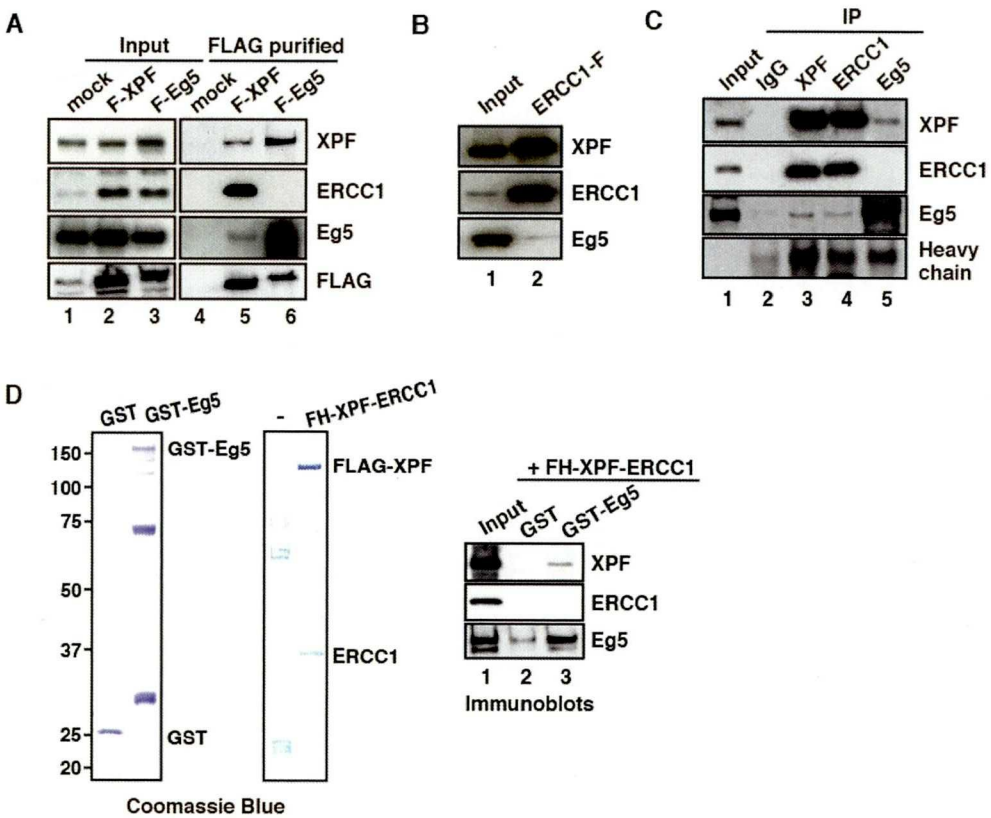
A
Input
FLAG purified
mock
F-XPF
F-Eg5
mock
F-XPF
F-Eg5
XPF
ERCC1
Eg5
FLAG
1 2 3 4 5 6
B
Input
ERCC1-F
XPF
ERCC1
Eg5
1 2
C
IP
Input
IgG
XPF
ERCC1
Eg5
XPF
ERCC1
Eg5
Heavy chain
1 2 3 4 5
D
GST
GST-Eg5
-
FH-XPF-ERCC1
150
100
75
50
37
25
20
GST-Eg5
FLAG-XPF
ERCC1
GST
Coomassie Blue
+ FH-XPF-ERCC1
Input
GST
GST-Eg5
XPF
ERCC1
Eg5
1 2 3
Immunoblots

Figure 3

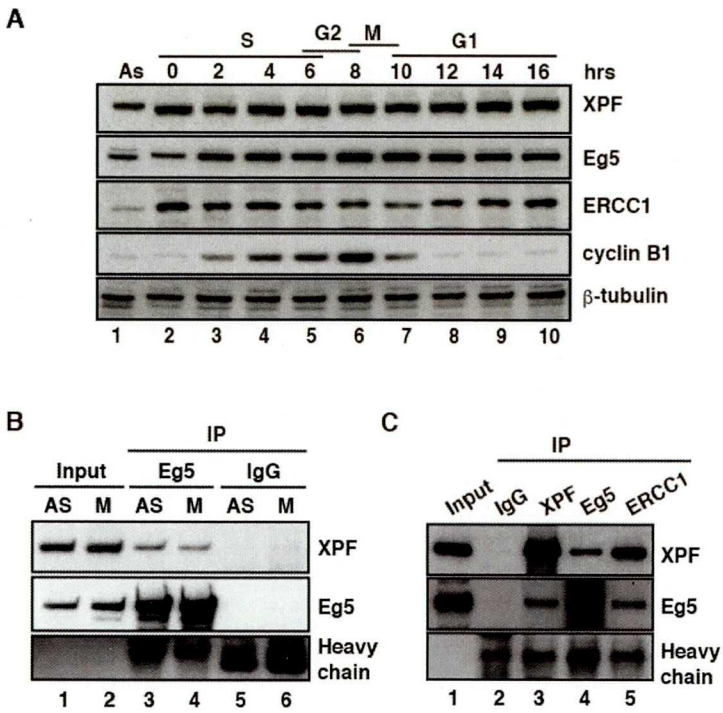
A
S
G2
M
G1
As 0 2 4 6 8 10 12 14 16 hrs
XPF
Eg5
ERCC1
cyclin B1
β-tubulin
1 2 3 4 5 6 7 8 9 10
B
IP
Input
Eg5
IgG
AS M AS M AS M
XPF
Eg5
Heavy chain
1 2 3 4 5 6
C
IP
Input
IgG
XPF
Eg5
ERCC1
XPF
Eg5
Heavy chain
1 2 3 4 5

Figure 4

A

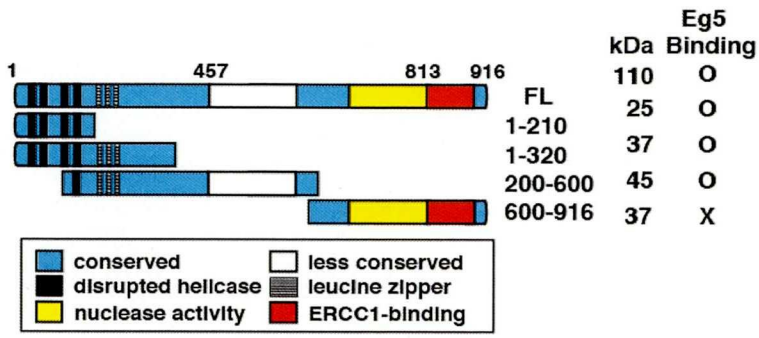
1
457
813
916
FL
1-210
1-320
200-600
600-916
kDa
Eg5 Binding
110 O
25 O
37 O
45 O
37 X
conserved
disrupted helicase
nuclease activity
less conserved
leucine zipper
ERCC1-binding

B

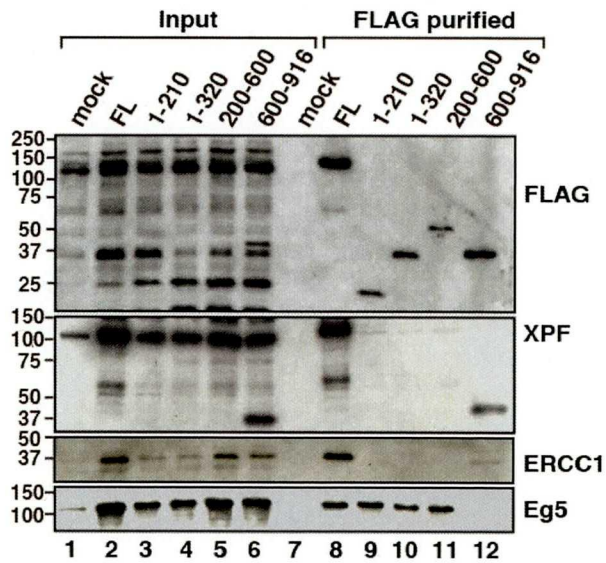
Input
FLAG purified
mock
FL
1-210
1-320
200-600
600-916
250
150
100
75
50
37
25
FLAG
XPF
ERCC1
Eg5
1 2 3 4 5 6 7 8 9 10 11 12

C

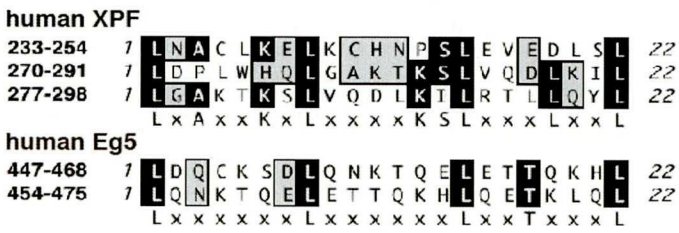
human XPF
233-254
270-291
277-298
human Eg5
447-468
454-475

Figure 5

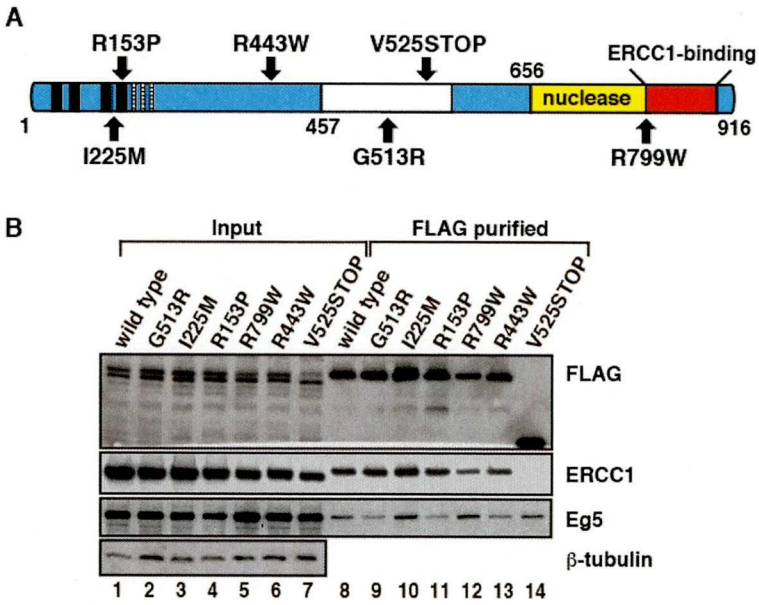

Table 2. Clinical features of XP-F patients and mutations

Mutation	Patient	Age	Clinical features	
I225M G513R	XP101OS*	49	mild XP basal cell epithelioma	mild
T567A 657fs	XP2YO*	65	mild XP squamous cell carcinoma	
R799W	XP42RO°	62	mild XP squamous cell carcinoma	
V525STOP R433W	XP42KY*	48	mental retardation cerebellar ataxia	
R153P	XP51RO°	16	neurodegeneration progeria (deceased)	severe

° homozygous
* heterozygous

Figure 6

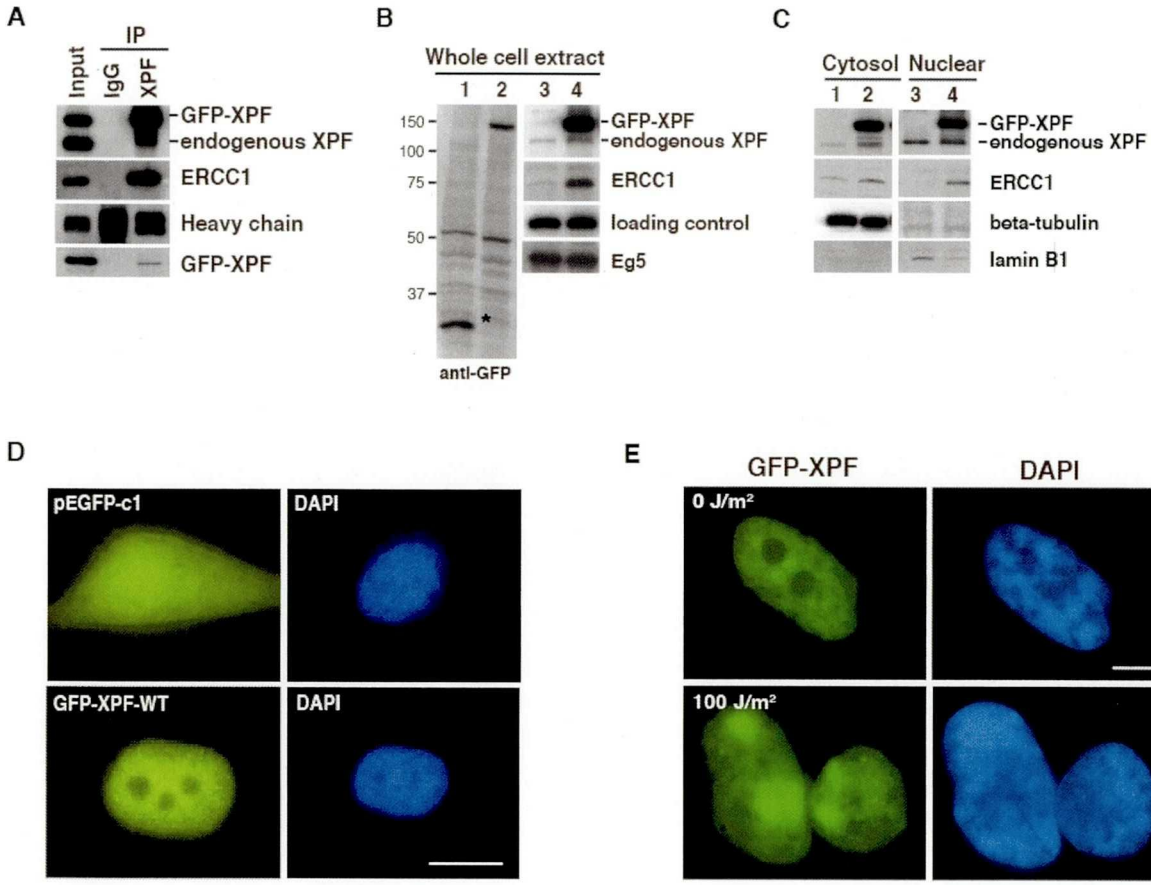
A
IP
Input
IgG
XPF
GFP-XPF
endogenous XPF
ERCC1
Heavy chain
GFP-XPF
B
Whole cell extract
1 2 3 4
150
100
75
50
37
*
anti-GFP
GFP-XPF
endogenous XPF
ERCC1
loading control
Eg5
C
Cytosol Nuclear
1 2 3 4
GFP-XPF
endogenous XPF
ERCC1
beta-tubulin
lamin B1
D
pEGFP-c1
DAPI
GFP-XPF-WT
DAPI
E
GFP-XPF
DAPI
0 J/m²
100 J/m²

Figure 7

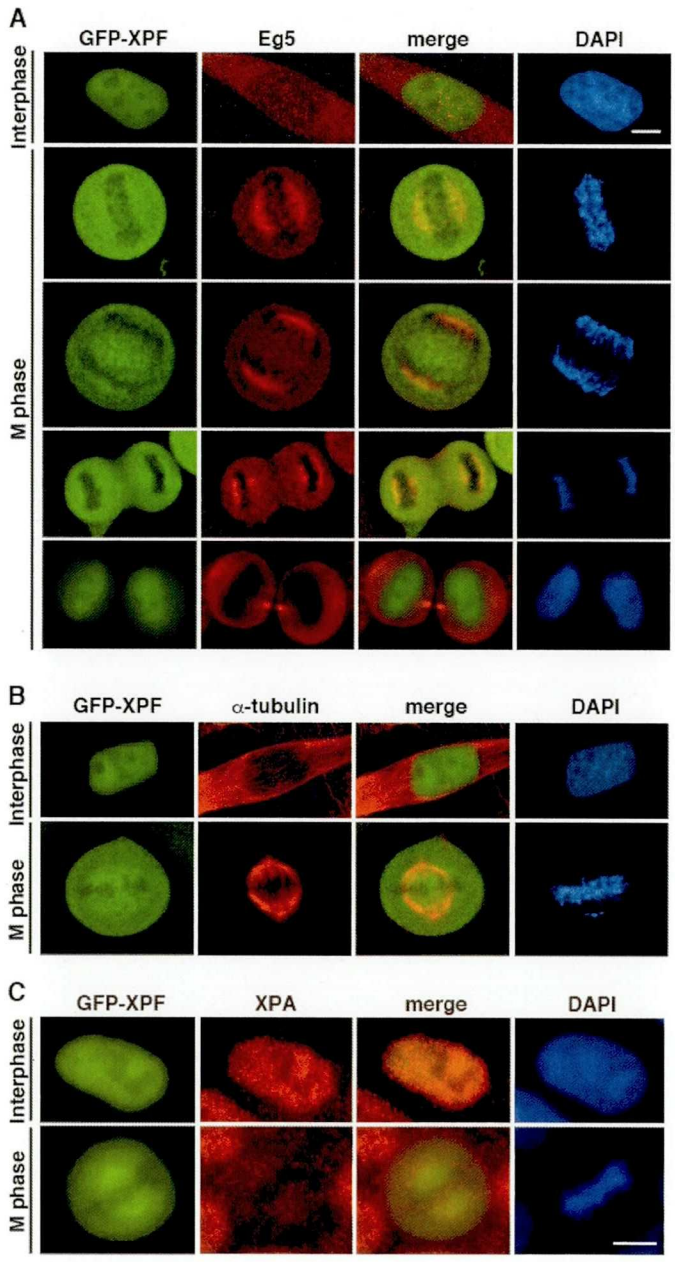
A
GFP-XPF
Eg5
merge
DAPI
Interphase
M phase
B
GFP-XPF
α-tubulin
merge
DAPI
Interphase
M phase
C
GFP-XPF
XPA
merge
DAPI
Interphase
M phase

Figure 8

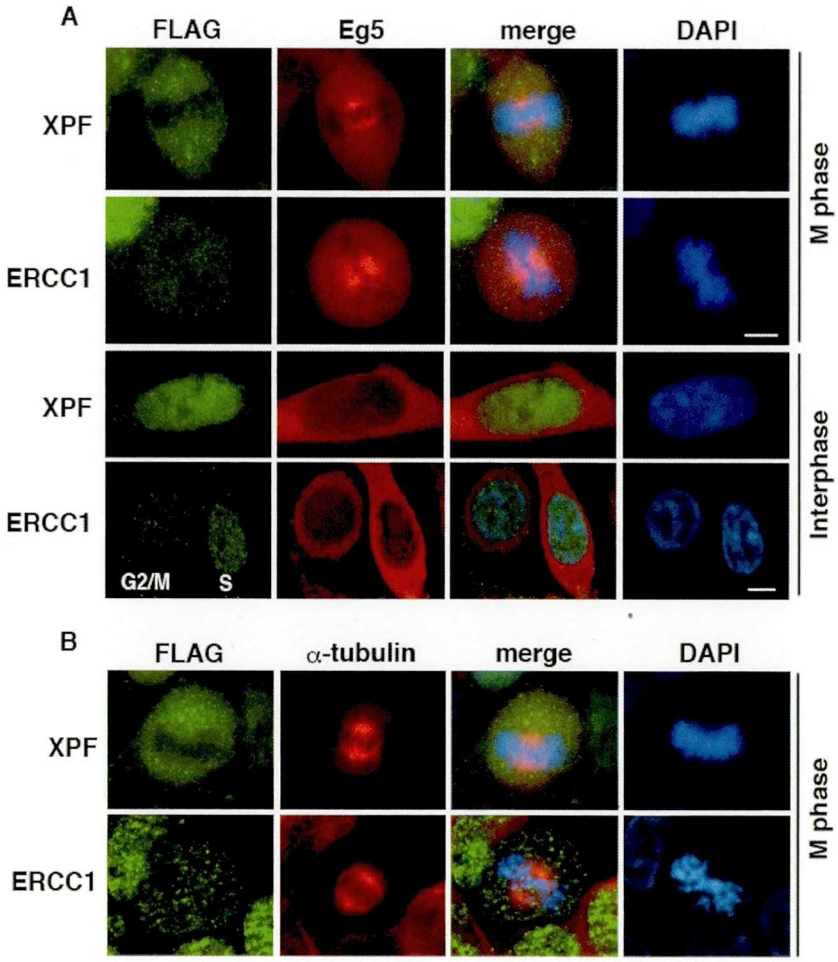
A
FLAG
Eg5
merge
DAPI
XPF
ERCC1
XPF
ERCC1
G2/M
S
M phase
Interphase
B
FLAG
α-tubulin
merge
DAPI
XPF
ERCC1
M phase

Figure 9

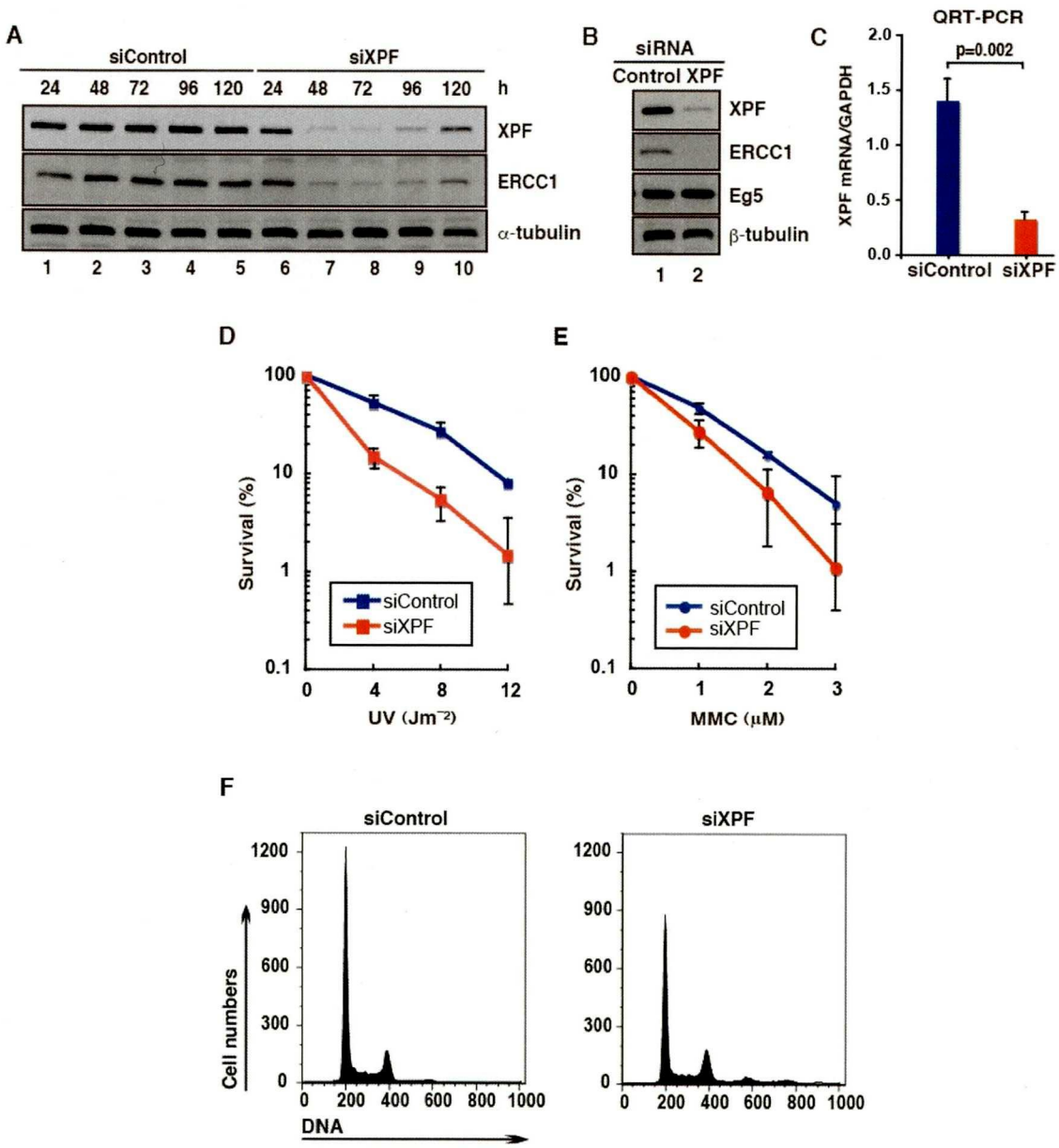
A
siControl
siXPF
24 48 72 96 120 24 48 72 96 120 h
XPF
ERCC1
α-tubulin
1 2 3 4 5 6 7 8 9 10
B
siRNA
Control XPF
XPF
ERCC1
Eg5
β-tubulin
1 2
C
QRT-PCR
p=0.002
XPF mRNA/GAPDH
2.0
1.5
1.0
0.5
0.0
siControl siXPF
D
Survival (%)
100
10
1
0.1
siControl
siXPF
0 4 8 12
UV (Jm⁻²)
E
Survival (%)
100
10
1
0.1
siControl
siXPF
0 1 2 3
MMC (μM)
F
siControl
siXPF
Cell numbers
1200
900
600
300
0
0 200 400 600 800 1000
DNA

Figure 10

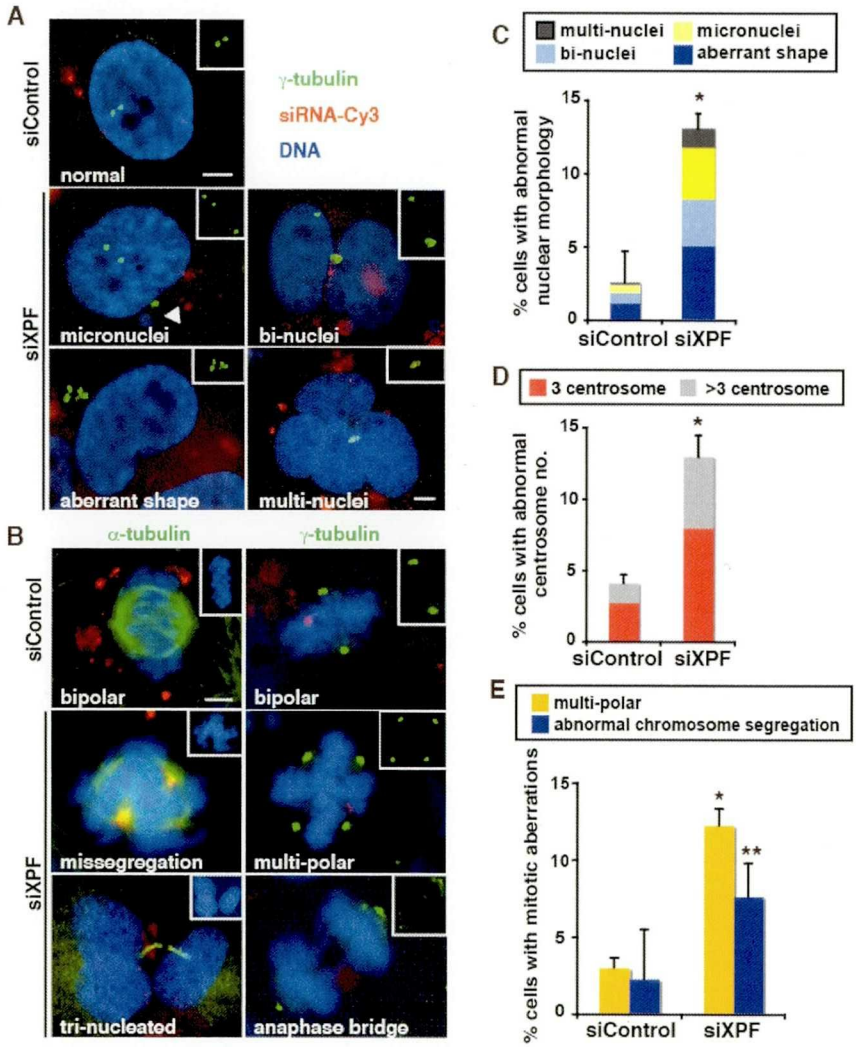
A
siControl
normal
γ-tubulin
siRNA-Cy3
DNA
siXPF
micronuclei
bi-nuclei
aberrant shape
multi-nuclei
B
α-tubulin
γ-tubulin
siControl
bipolar
bipolar
siXPF
missegregation
multi-polar
tri-nucleated
anaphase bridge
C
multi-nuclei
micronuclei
bi-nuclei
aberrant shape
% cells with abnormal nuclear morphology
15
10
5
0
*
siControl siXPF
D
3 centrosome
>3 centrosome
% cells with abnormal centrosome no.
15
10
5
0
*
siControl siXPF
E
multi-polar
abnormal chromosome segregation
% cells with mitotic aberrations
15
10
5
0
*
**
siControl siXPF

Figure 11

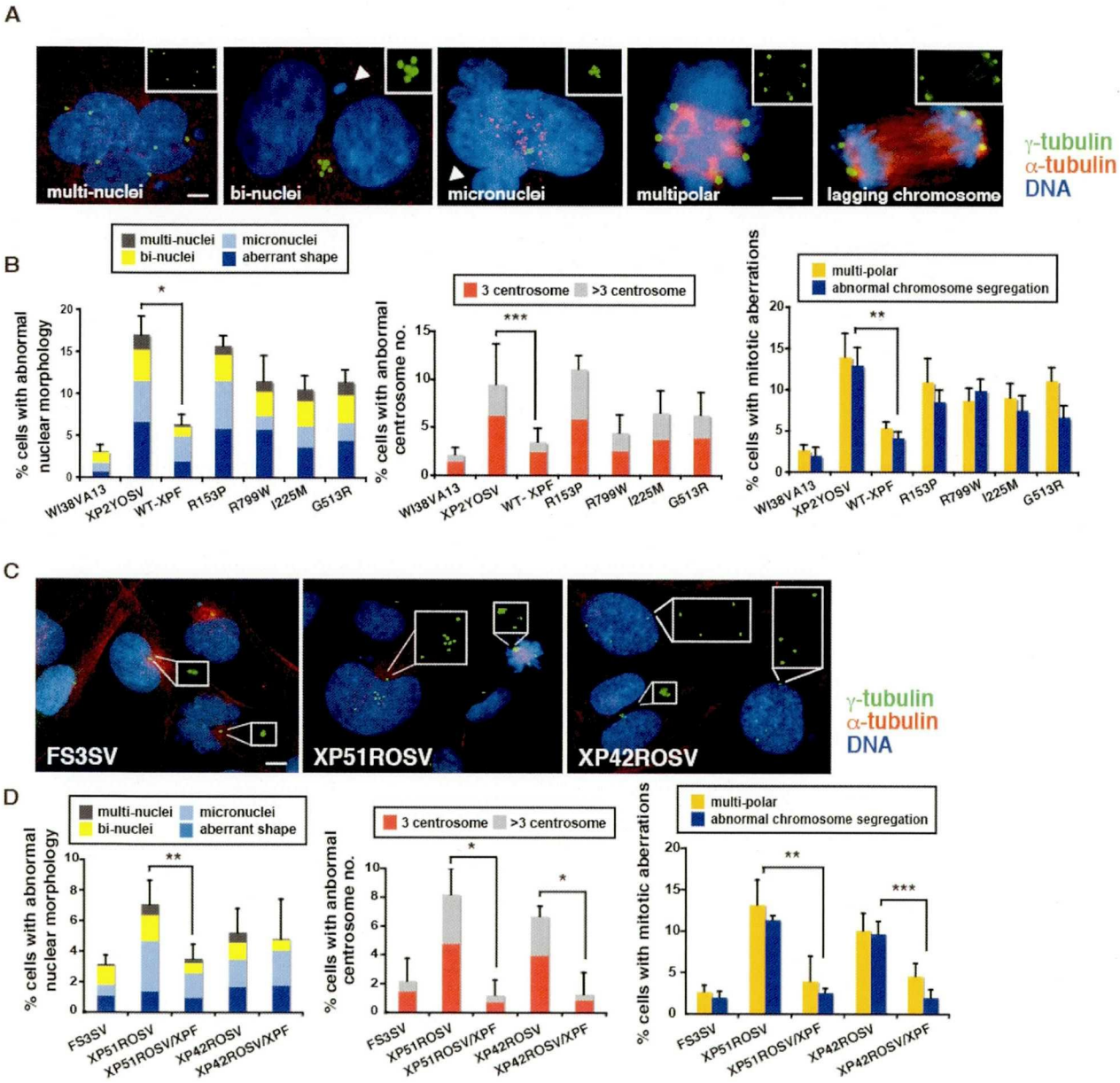
A
multi-nuclei
bi-nuclei
micronuclei
multipolar
lagging chromosome
γ-tubulin
α-tubulin
DNA
B
multi-nuclei
bi-nuclei
micronuclei
aberrant shape
% cells with abnormal nuclear morphology
3 centrosome
>3 centrosome
% cells with anbormal centrosome no.
multi-polar
abnormal chromosome segregation
% cells with mitotic aberrations
WI38VA13
XP2YOSV
WT-XPF
R153P
R799W
I225M
G513R
C
FS3SV
XP51ROSV
XP42ROSV
γ-tubulin
α-tubulin
DNA
D
FS3SV
XP51ROSV
XP51ROSV/XPF
XP42ROSV
XP42ROSV/XPF

Figure 12

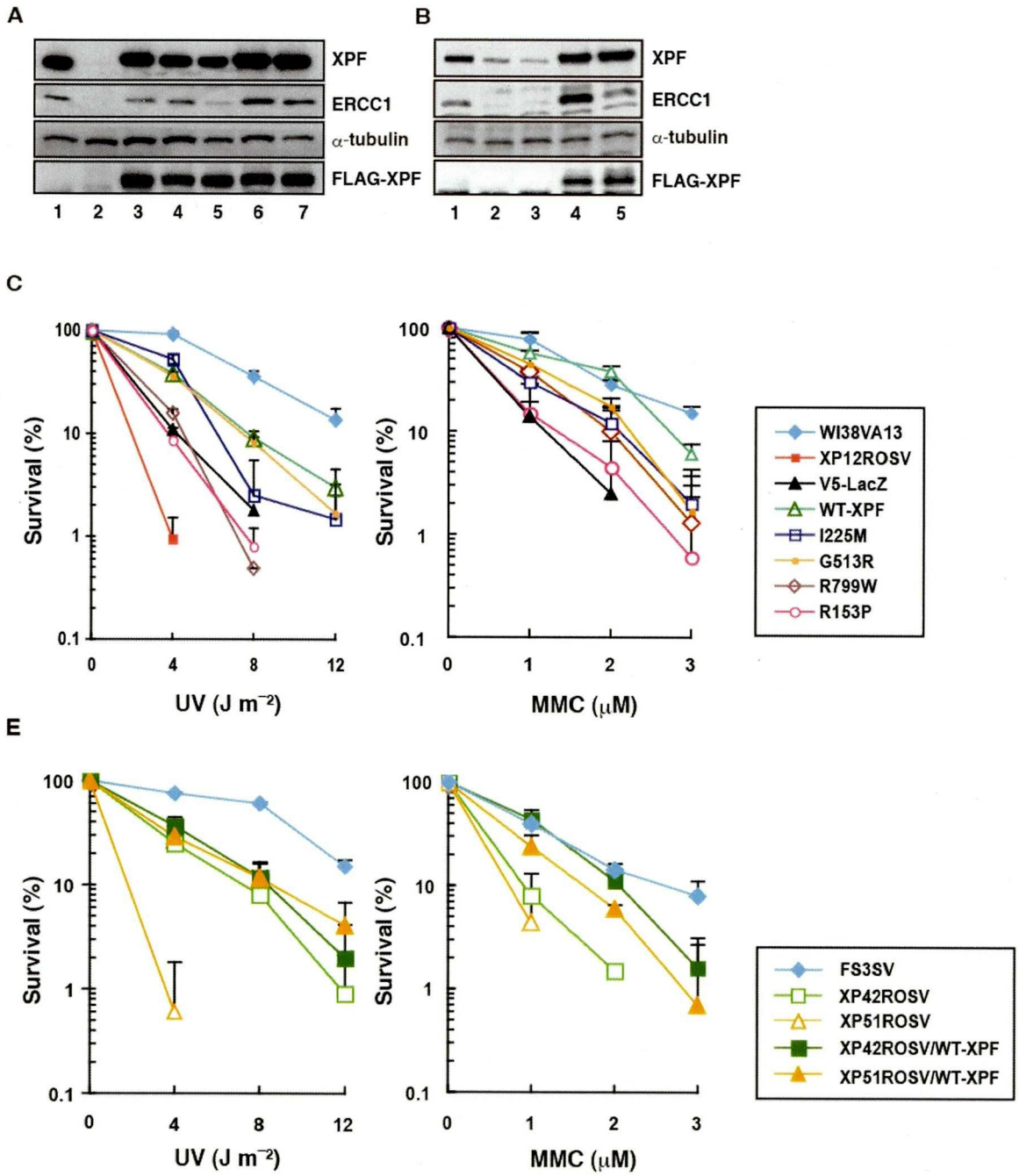
A
XPF
ERCC1
α-tubulin
FLAG-XPF
1 2 3 4 5 6 7
B
XPF
ERCC1
α-tubulin
FLAG-XPF
1 2 3 4 5
C
Survival (%)
100
10
1
0.1
0 4 8 12
UV (J m⁻²)
0 1 2 3
MMC (μM)
WI38VA13
XP12ROSV
V5-LacZ
WT-XPF
I225M
G513R
R799W
R153P
E
Survival (%)
UV (J m⁻²)
MMC (μM)
FS3SV
XP42ROSV
XP51ROSV
XP42ROSV/WT-XPF
XP51ROSV/WT-XPF